



**HAL**  
open science

# A Framework for Estimating Global River Discharge From the Surface Water and Ocean Topography Satellite Mission

Michael Durand, Colin J Gleason, Tamlin M Pavelsky, Renato Prata de Moraes Frasson, Michael Turmon, Cédric H David, Elizabeth H Altenau, Nikki Tebaldi, Kevin Larnier, Jerome Monnier, et al.

## ► To cite this version:

Michael Durand, Colin J Gleason, Tamlin M Pavelsky, Renato Prata de Moraes Frasson, Michael Turmon, et al.. A Framework for Estimating Global River Discharge From the Surface Water and Ocean Topography Satellite Mission. *Water Resources Research*, 2023, 59 (4), 10.1029/2021wr031614 . hal-04105447

**HAL Id: hal-04105447**

**<https://hal.inrae.fr/hal-04105447>**

Submitted on 24 May 2023

**HAL** is a multi-disciplinary open access archive for the deposit and dissemination of scientific research documents, whether they are published or not. The documents may come from teaching and research institutions in France or abroad, or from public or private research centers.

L'archive ouverte pluridisciplinaire **HAL**, est destinée au dépôt et à la diffusion de documents scientifiques de niveau recherche, publiés ou non, émanant des établissements d'enseignement et de recherche français ou étrangers, des laboratoires publics ou privés.



Distributed under a Creative Commons Attribution - NonCommercial 4.0 International License

# Water Resources Research



## RESEARCH ARTICLE

10.1029/2021WR031614

## A Framework for Estimating Global River Discharge From the Surface Water and Ocean Topography Satellite Mission

### Key Points:

- The Surface Water and Ocean Topography satellite mission is designed to enable the estimation of discharge for global rivers wider than 100 m
- When unconstrained by in situ data, discharge uncertainty is expected to be <30% for most reaches, and to be dominated by systematic bias
- We expect discharge temporal variations to be estimated to within 15% for nearly all reaches globally

Michael Durand<sup>1</sup> , Colin J. Gleason<sup>2</sup> , Tamlin M. Pavelsky<sup>3</sup> , Renato Prata de Moraes Frasson<sup>4</sup> , Michael Turmon<sup>4</sup>, Cédric H. David<sup>4</sup> , Elizabeth H. Altenau<sup>3</sup> , Nikki Tebaldi<sup>4</sup> , Kevin Larnier<sup>5</sup> , Jerome Monnier<sup>6</sup>, Pierre Olivier Malaterre<sup>7</sup> , Hind Oubanas<sup>7</sup>, George H. Allen<sup>8</sup> , Brian Astifan<sup>9</sup>, Craig Brinkerhoff<sup>2</sup>, Paul D. Bates<sup>10</sup> , David Bjerklie<sup>11</sup> , Stephen Coss<sup>1</sup> , Robert Dudley<sup>11</sup> , Luciana Fenoglio<sup>12</sup> , Pierre-André Garambois<sup>13</sup>, Augusto Getirana<sup>14,15</sup>, Peirong Lin<sup>16</sup> , Steven A. Margulis<sup>17</sup> , Pascal Matte<sup>18</sup> , J. Toby Minear<sup>19</sup> , Aggrey Muhebwa<sup>20</sup> , Ming Pan<sup>21</sup>, Daniel Peters<sup>18</sup>, Ryan Riggs<sup>22</sup> , Md Safat Sikder<sup>20</sup>, Travis Simmons<sup>2</sup>, Cassie Stuurman<sup>4</sup>, Jay Taneja<sup>20</sup>, Angelica Tarpanelli<sup>23</sup> , Kerstin Schulze<sup>12</sup> , Mohammad J. Tourian<sup>24</sup> , and Jida Wang<sup>20</sup> 

<sup>1</sup>School of Earth Sciences, and Byrd Polar and Climate Research Center, The Ohio State University, Columbus, OH, USA, <sup>2</sup>Department of Civil and Environmental Engineering, University of Massachusetts Amherst, Amherst, MA, USA, <sup>3</sup>Department of Geological Sciences, University of North Carolina, Chapel Hill, NC, USA, <sup>4</sup>Jet Propulsion Laboratory, California Institute of Technology, Pasadena, CA, USA, <sup>5</sup>Space Department, CS Corporation, Toulouse, France, <sup>6</sup>INSA Toulouse—Math. Institute of Toulouse (IMT), Toulouse, France, <sup>7</sup>G-EAU, Univ Montpellier, AgroParisTech, BRGM, CIRAD, IRD, INRAE, Institut Agro, Montpellier, France, <sup>8</sup>Department of Geosciences, Virginia Polytechnic Institute and State University, Blacksburg, VA, USA, <sup>9</sup>Ohio River Forecast Center, NOAA NWS, Wilmington, OH, USA, <sup>10</sup>School of Geographical Sciences, University of Bristol, Bristol, UK, <sup>11</sup>New England Water Science Center, U.S. Geological Survey, Northborough, MA, USA, <sup>12</sup>Department of Geodesy and Geoinformation, University of Bonn, Bonn, Germany, <sup>13</sup>INRAE, RECOVER, Aix-Marseille University, Marseille, France, <sup>14</sup>Hydrological Sciences Laboratory, NASA Goddard Space Flight Center, Greenbelt, MD, USA, <sup>15</sup>Science Applications International Corporation, Greenbelt, MD, USA, <sup>16</sup>School of Earth and Space Sciences, Institute of Remote Sensing and GIS, Peking University, Beijing, China, <sup>17</sup>Department of Civil and Environmental Engineering, UCLA, Los Angeles, CA, USA, <sup>18</sup>Science and Technology Branch, Environment and Climate Change Canada, Canada, QC, Canada, <sup>19</sup>Cooperative Institute for Research in Environmental Sciences, University of Colorado Boulder, Boulder, CO, USA, <sup>20</sup>Department of Geography and Geospatial Sciences, Kansas State University, Manhattan, KS, USA, <sup>21</sup>Center for Western Weather and Water Extremes, Scripps Institution of Oceanography, University of California San Diego, La Jolla, CA, USA, <sup>22</sup>Department of Geography, Texas A&M University, College Station, TX, USA, <sup>23</sup>Research Institute for Geo-Hydrological protection, National Research Council, Perugia, Italy, <sup>24</sup>Institute of Geodesy, University of Stuttgart, Stuttgart, Germany

### Correspondence to:

S. Coss,  
coss.31@osu.edu

### Citation:

Durand, M., Gleason, C. J., Pavelsky, T. M., Prata de Moraes Frasson, R., Turmon, M., David, C. H., et al. (2023). A framework for estimating global river discharge from the Surface Water and Ocean Topography satellite mission. *Water Resources Research*, 59, e2021WR031614. <https://doi.org/10.1029/2021WR031614>

Received 22 NOV 2021  
Accepted 18 MAR 2023  
Corrected 20 APR 2023

This article was corrected on 20 APR 2023. See the end of the full text for details.

**Abstract** The Surface Water and Ocean Topography (SWOT) mission will vastly expand measurements of global rivers, providing critical new data sets for both gaged and ungaged basins. SWOT discharge products (available approximately 1 year after launch) will provide discharge for all river that reaches wider than 100 m. In this paper, we describe how SWOT discharge produced and archived by the US and French space agencies will be computed from measurements of river water surface elevation, width, and slope and ancillary data, along with expected discharge accuracy. We present for the first time a complete estimate of the SWOT discharge uncertainty budget, with separate terms for random (standard error) and systematic (bias) uncertainty components in river discharge time series. We expect that discharge uncertainty will be less than 30% for two-thirds of global reaches and will be dominated by bias. Separate river discharge estimates will combine both SWOT and in situ data; these “gage-constrained” discharge estimates can be expected to have lower systematic uncertainty. Temporal variations in river discharge time series will be dominated by random error and are expected to be estimated within 15% for nearly all reaches, allowing accurate inference of event flow dynamics globally, including in ungaged basins. We believe this level of accuracy lays the groundwork for SWOT to enable breakthroughs in global hydrologic science.

**Plain Language Summary** The Surface Water and Ocean Topography (SWOT) satellite mission was launched on 15 December 2022. SWOT is designed to produce estimates of river discharge on many rivers where no in situ discharge measurements are currently available. This paper describes how SWOT discharge estimates will be created, and their expected accuracy. SWOT discharge will be estimated using simple flow laws that combine SWOT measurements of river water elevation above sea level, river width, and river slope, with ancillary data such as river bathymetry. We expect that discharge uncertainty will be less than 30% for

© 2023 The Authors.

This is an open access article under the terms of the [Creative Commons Attribution-NonCommercial License](https://creativecommons.org/licenses/by-nc/4.0/), which permits use, distribution and reproduction in any medium, provided the original work is properly cited and is not used for commercial purposes.

two-thirds of global reaches and will be dominated by a systematic bias. Temporal variations in river discharge time series are expected to be estimated within 15% for nearly all reaches, thus capturing the response of river discharge to rainfall and snowmelt events, including in basins that are currently ungaged, and providing a new capability for scientists to better track the flows of freshwater water through the Earth system.

## 1. Introduction

Launched on 15 December 2022, the Surface Water and Ocean Topography (SWOT) satellite enables estimates of global river discharge, vastly increasing the observational basis for understanding global hydrological processes (Biancamaria et al., 2016). Measurements of river discharge integrate upstream water cycle processes, and thus are among our most important data resources for understanding hydrology from the watershed to continental scales. However, most of the world's rivers are functionally ungaged due to a range of factors including lack of resources and lack of data sharing (Gleason & Hamdan, 2017; Hannah et al., 2011). Remote sensing of river discharge provides the possibility of global observation even in ungaged basins, but with important tradeoffs, including decreased measurement accuracy, precision, and sampling frequency as compared with observing discharge in situ (Gleason & Durand, 2020). SWOT is a collaboration between the space agencies of the United States, France, United Kingdom, and Canada, and will measure oceans and surface water. SWOT measurements of river water surface elevation (WSE), top width and longitudinal water surface slope (JPL Internal Document, 2020) enable SWOT discharge estimates, allowing potential global scale advances in hydrology. A benchmarking study recently focused on one aspect of expected performance of algorithms used to estimate SWOT discharge in ungaged basins (Frasson et al., 2021). However, a full exploration of SWOT discharge philosophy, methodology, and expected uncertainty has not been presented in the literature.

The purpose of this paper is to document SWOT discharge creation, space-time coverage, and expected precision and accuracy for the hydrologic community. We first note that SWOT discharge is not monolithic—open satellite data will allow for many “SWOT Discharge” products created by hydrologists across the scientific community. This paper is therefore primarily concerned with the SWOT discharge to be archived and distributed by the US and French space agencies (referred to as the “Agency” discharge estimates). We first describe the philosophy behind the SWOT discharge (Section 2), and data sets used to produce SWOT discharge (Section 3), including SWOT observations and ancillary measurements. We then describe how SWOT discharge will be produced (Section 4) and expected accuracy (Section 5), relating expected SWOT discharge accuracy with that achievable from in situ measurements. Our aim is to describe SWOT discharge characteristics before their availability, thus maximizing hydrologic science returns from SWOT.

## 2. SWOT Discharge Philosophy

To understand the SWOT discharge products, it is helpful to begin with an appreciation of the challenges that must be overcome to estimate river discharge globally. These challenges have led to data product decisions that together constitute a philosophy for SWOT discharge. Whereas previous papers on SWOT discharge and related efforts have predominantly described methodological advances, here we bring together these challenges and the resulting philosophy in a single place.

Discharge is a critical part of the SWOT mission, but not all the information needed to compute discharge is directly available from the SWOT measurements. Discharge is specified as a required product to be produced and distributed by the space agencies in the SWOT science requirements document, the foundational mission document that specifies what SWOT products must be produced and with what accuracy (JPL Internal Document, 2018). SWOT measurements of rivers include WSE, river width, and slope, each of which is invaluable in estimating river discharge (for further information on SWOT measurements; see Section 3.2). However, these measurements together do not have a unique relationship to river discharge. Thus, the SWOT Science Team will develop and deploy methods to estimate the additional properties of global rivers needed to produce the Agency discharge estimate. (Note that SWOT, like many large satellite missions, has a “Science Team” comprised of researchers from around the globe to support the mission.) The Science Team will likely create and distribute additional discharge data products: see Section 4.7 for details. The Agency discharge estimates are thus a partnership between the Agencies and the Science Team.

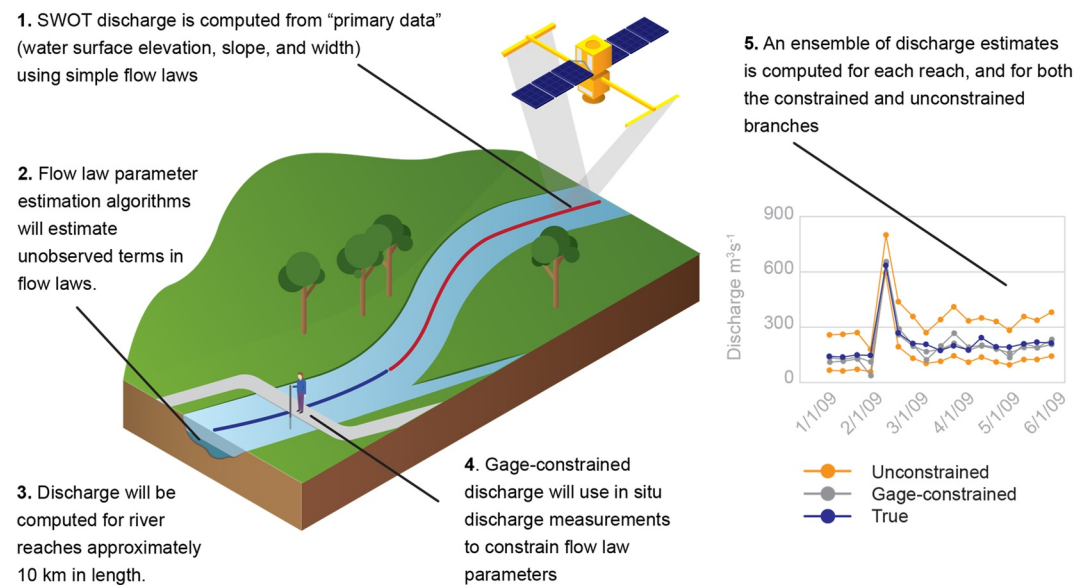


**Figure 1.** The five points numbered in the figure correspond to the five points governing Agency discharge products. The blue and red lines in the cartoon illustrate two conceptual river reaches. The hydrographs on the right-hand side of the figure are derived from simulated Surface Water and Ocean Topography (SWOT) observations (Frasson et al., 2017) on the Sacramento River. “Consensus” discharge estimates (see text for description) are not shown.

The philosophy and corresponding methods used to produce SWOT discharge are shaped by the nature of the SWOT measurements, and the need to apply SWOT to estimate discharge in ungaged basins. SWOT discharge methods thus differ from the well-known two-step process to estimate river discharge at in situ gages (Turnipseed & Sauer, 2010). In this traditional approach, gage discharge is estimated by first establishing a “rating curve” by making joint measurements of river stage (height above an arbitrary datum) and river discharge; the latter is obtained by measuring the river velocity profile at a river cross-section with either a current meter or an Acoustic Doppler Current Profiler (ADCP). Second, once the rating curve is established, discharge is predicted from the rating curve via continuous observations of river stage, typically measured by a pressure transducer. SWOT discharge will also be estimated by a two-step process that is an analog to gages: In the first step, we establish a relationship between SWOT observations and river discharge, and in the second step, SWOT observations are used along with the relationship to estimate discharge on each SWOT overpass. However, the methodological details for the first step differ significantly from the rating curve calibration approach due to the lack of in situ discharge data for most of the world. As noted earlier, this article focuses on the SWOT discharge produced by the space agencies (JPL Internal Document, 2020), which follows this two-step methodology; see Section 4.7 for other approaches to SWOT discharge. The philosophy governing Agency discharge products can be summarized in five points (Figure 1); note that these are five philosophical points, rather than five sequential steps in discharge estimation.

First, river discharge estimates will be driven by “primary data,” defined by Gleason and Durand (2020) as “electromagnetic radiation recorded directly by the satellite.” Thus, the basic form of flow laws used to compute discharge ( $Q_t$ ) for each reach and for each SWOT overpass at a time  $t$  must rely on SWOT observations, and will in most cases be a modified form of the Gauckler-Manning-Strickler equation (referred to as the “modified Manning’s equation,” hereafter):

$$Q_t = \frac{1}{n_t} (\bar{A} + A'_t)^{5/3} W_t^{-2/3} S_t^{1/2}, \quad (1)$$

where  $n_t$  is the coefficient governing hydraulic resistance in the river,  $\bar{A}$  is the time-series median cross-sectional area (note that  $n_t$  and  $\bar{A}$  are computed as described below),  $A'_t$  is the cross-sectional area anomaly (i.e., the time-varying part), such that  $\bar{A} + A'_t$  estimates the total cross-sectional area at time  $t$ ,  $W_t$  and  $S_t$  are SWOT observations of reach averaged river width and surface slope, respectively, and the  $t$  subscript denotes values that vary

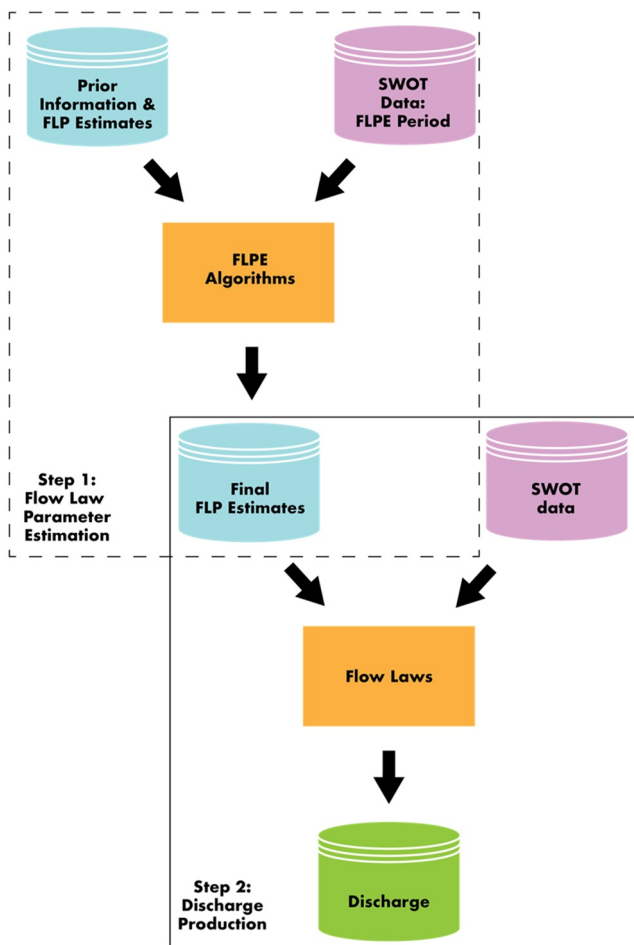


**Figure 2.** Summary of the two steps of Surface Water and Ocean Topography (SWOT) discharge production. In step 1 (denoted by the dashed line box in the figure), flow law parameters (FLPs) are estimated by the Science Team. In step 2 (denoted by the solid line box) discharge is produced using the estimated flow law parameters, and SWOT observations. FLPE is flow law parameter estimation.

from pass to pass (note that all quantities vary spatially). See Appendix A for details of the derivation of Equation 1 and see Section 3.2 for SWOT observation precision and spatial and temporal sampling characteristics. We assert that  $A_i$  is measured by SWOT, as it is computed in a straightforward way from SWOT WSE and river width observations (see Appendix A). Values of  $n_i$  are computed from simple functions of SWOT observations as described in Section 4.2. All quantities in Equation 1 are reach averages. Equation 1 is derived from the shallow water equations under simplifying assumptions as described in Section 4.2. Discharge computations from these simple flow laws enable straightforward uncertainty quantification (see Section 5) and meet the practical requirement that global discharge computation proceed with little or no supervision by the space agencies. As discharge is predicted from these flow laws, SWOT does not “measure” discharge but rather “estimates” it. SWOT discharge estimates are thus driven by primary data in that time variations in discharge are driven only by time variations in the remote sensing observations of WSE, width, and slope.

Second, as described earlier in this section, discharge will be computed using a two-step process: members of the SWOT Science Team will compute optimal estimates of flow law parameters, then provide these to the space agencies for regular computation of SWOT discharge using the chosen flow laws (Figure 2). This two-step process is necessary because SWOT cannot measure all flow law terms, such as the coefficient governing hydraulic resistance and the river bathymetry (represented by  $n_i$  and  $\bar{A}$  respectively, in Equation 1). These unobserved terms in the flow laws are referred to as “flow law parameters” (FLPs) hereafter. FLP estimates will be computed by the Science Team after SWOT data is available using algorithms described in Section 4.3. After FLPs are estimated, SWOT discharge will be produced automatically for each SWOT pass. These two steps are referred to as “flow law parameter estimation” (FLPE) and “discharge production.”

Third, SWOT discharge will be produced reaching approximately 10 km in length. The selection of 10 km as the reach length was driven by precision of reach averaged WSE, width, and slope measurements. SWOT WSE measurements will be noisy at the scale of individual radar pixels (JPL Internal Document, 2017). Rodriguez et al. (2020) showed that averaging to reaches of approximately 10 km is necessary to resolve river features. Thus, the Agency discharge products will be produced at reach scale; reach averaging necessitates adaptation of flow laws, as shown by Rodriguez et al. (2020),

and discussed in Section 4.2. We control for changes in discharge within the reach by choosing reaches to avoid major confluences: see Section 3.1. Reach definition takes into account low-head dams and other river obstructions (X. Yang et al., 2022). Possible Science Team discharge estimates at higher spatial resolution are discussed in Section 4.7.

Fourth, two branches of SWOT discharge will be produced: one where in situ data are used to constrain SWOT discharge, and one where in situ data are not used to constrain discharge, referred to as “gauge constrained” and “unconstrained,” respectively. Philosophically, these two branches are driven by the fact that SWOT discharge estimates will be used in both gaged and ungaged basins, with different sets of expectations and requirements regarding discharge accuracy. For example, most remotely sensed precipitation estimates are constrained to precipitation gages, where these are available (Hou et al., 2014), providing precedent for constraining SWOT remote sensing of discharge to stream gage data. The constrained branch will leverage both historical and concurrent gaged discharge data. A priori information (e.g., mean annual flow predicted by global hydrological models) will still be used to “inform” the unconstrained products. This is in accordance with our philosophy because methods to estimate “unconstrained” FLPs use model data only as a priori information in the Bayesian sense, and, the models used (e.g., the Water Balance Model [WBM] described by Cohen et al. (2014)) are not themselves calibrated on in situ discharge data. Parameter estimates are Bayesian in that they weight prior estimates

of mean annual flow or river geomorphology against information derived from inverse algorithms, based on their respective uncertainties (Hagemann et al., 2017). In contrast, the “gage constrained” FLPs will be chosen assuming the availability of suitable in situ discharge data and informed by global models calibrated at specific gage sites. Gage discharge will be used only during the calculation of the FLPs, not during the operational discharge calculation by space agencies. Additionally, some discharge gages will be reserved for validation purposes (i.e., not used to constrain either prior models or SWOT discharge) to assess discharge accuracy and precision of both the gage-constrained and unconstrained products (see Section 4.5, below).

Fifth, Agency products will include an ensemble of discharge estimates, produced using several different flow laws and FLPE algorithms described in Section 4.3. A “consensus” discharge estimate based on a summary statistic computed across the ensemble will also be included (see Section 4.4). This ensemble approach is driven by the fact that FLPE in ungaged basins is challenging, and it is unlikely that a single approach is optimal for all rivers. The ensemble approach adds robustness to SWOT discharge.

### 3. Data and Data Sets Used for SWOT Discharge Estimation

In this section, we describe the SWOT mission river database (SWORD; Section 3.1), SWOT observations (Section 3.2), and ancillary data (Section 3.3) used for FLPE and discharge production.

#### 3.1. SWOT Mission River Database

SWORD archives both spatial data and reaches attributes for SWOT reaches (Altenau et al., 2021) and is critical to the creation of SWOT river data products. The primary spatial attributes of SWOT reaches are SWORD river centerlines, which are specified based on the Global River Widths from the Landsat data set (Allen & Pavelsky, 2018) at ~30 m spatial resolution, using Landsat data and the RivWidth algorithm (Pavelsky & Smith, 2008). SWORD also defines spatial data and attributes for river nodes, a series of points at approximately 200 m increments along river longitudinal profiles defined by the SWORD centerline. SWORD reaches and nodes are used in several stages of SWOT processing: for example, SWOT radar pixels are mapped onto SWORD node locations using the RiverObs software (<https://github.com/SWOTAlgorithms/RiverObs>), translating two-dimensional imagery to one-dimensional measurements of WSE, width, and slope. SWORD archives river ice climatology (derived following the methods of X. Yang et al. (2020)) used for SWOT ice flagging. SWORD distance from river outlet (also called “chainage”) and SWOT WSE at the node scale are combined to compute SWOT reach averaged river slope. SWORD also archives drainage area, extracted from data sets such as MERIT Hydro (Yamazaki et al., 2019), river topology, and river obstructions data from the Global River Obstruction Database (Whittemore et al., 2020). Once FLPs have been computed by the Science Team, they will be attached to SWORD for the Agencies to use in producing discharge estimates. See Altenau et al. (2021) for further details.

#### 3.2. SWOT Observations: Spatial and Temporal Sampling Characteristics, and Precision

SWOT WSE, width, and slope resolution and precision are relevant to methods used to calculate discharge, and so are briefly reviewed here; for more details, see the SWOT River Single Pass Product Description Document (JPL Internal Document, 2020) example data products (<https://podaac.jpl.nasa.gov/swot?tab=datasets>), Science Requirements Document (JPL Internal Document, 2018) and Mission Performance and Error Budget (JPL Internal Document, 2017). SWOT WSE is measured interferometrically, and is defined relative to the Earth Gravitational Model 2008 (EGM2008) geoid (Pavlis et al., 2012), where the geoid is the vertical distance above the World Geodetic System (WGS84) ellipsoid model of the Earth surface. SWOT width is computed as a reach average, by summing the inundated area of each SWOT radar pixel associated with a particular river reach and dividing by reach length (Frasson et al., 2017). Note that the SWOT mission has two phases, marked by different orbits and resulting spatiotemporal sampling. In the first phase (nominally 3 months long), SWOT measures a small subset of global rivers with daily sampling; this is the “fast repeat orbit.” In the second phase (nominally 3 years long), all rivers are covered with less frequent temporal sampling; this is the “nominal science orbit.” Only spatial and temporal sampling for the nominal science orbit is described here. The SWOT mission goal for latency is 3 days: in other words, data will likely be available 3 days after each satellite pass (note that discharge products will not be available beginning approximately 1 year after launch; see Section 4.5 for details).

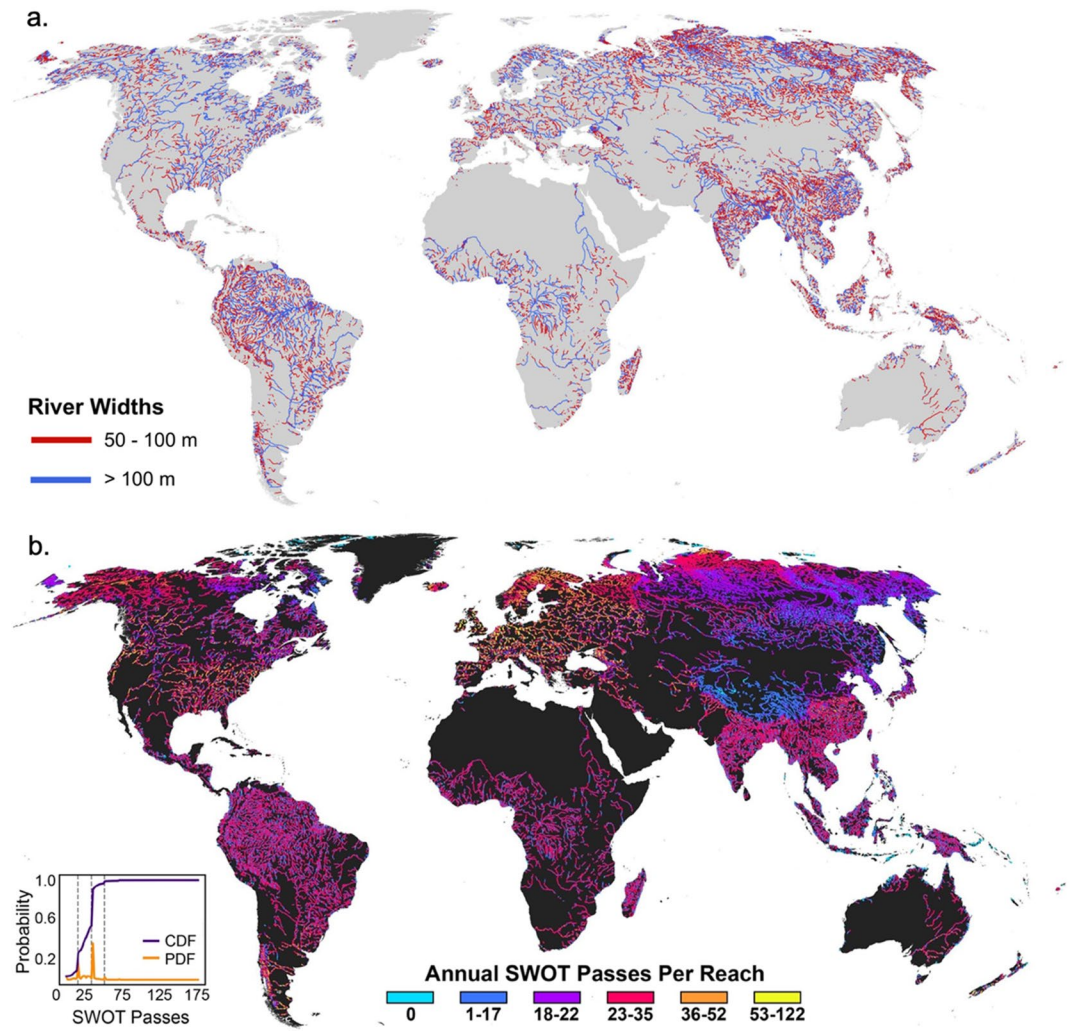


**Figure 3.** (a) Surface Water and Ocean Topography (SWOT) mission river database (SWORD) river reaches shown by whether they meet the width cutoff for required discharge production (100 m). (b) Total number of SWOT passes per year observed on each reach, globally for all river reaches in SWORD, including the effects of ice cover reduction in SWOT passes. The inset shows the empirical cumulative distribution (CDF) and histogram (PDF) of annual number of SWOT passes.

### 3.2.1. Spatial Characteristics

Figure 3a shows all rivers expected to be observed by SWOT based on SWORD (Altenau et al., 2021), broken out by width. The native resolution of the KaRIn radar on SWOT varies across the swath; the SWOT “pixel cloud” (from which SWOT river data products are computed) varies in resolution from 10 to 60 m in the cross-track direction and is posted every 20 m in the along-track direction. Many pixels are averaged together to compute river width, WSE, and slope (Frasson et al., 2017; JPL Internal Document, 2020). Some pixels measure both water and land, but because water is far brighter than land at SWOT incidence angles and at Ka-band, precise hydrologic information about relatively narrow rivers can be extracted from the SWOT measurements. The Science Requirements Document requires only that SWOT products be produced for rivers greater than 100 m, with a science goal of producing data products for all rivers wider than 50 m (JPL Internal Document, 2018). As shown by Pavelsky et al. (2014), SWOT spatial coverage assuming either 50 m or 100 m is far greater than current gage coverage. There are 213,485 SWORD river reaches, but many of these are too narrow, represent lakes or reservoirs that fall along rivers, are short reaches that span river obstructions, or are in areas of unreliable river topology; SWOT discharge will not be produced for such reaches. After filtering such reaches, a total of 62,809 reaches are wider than 100 m, and a total of 122,684 reaches are wider than 50 m. SWOT discharge will be

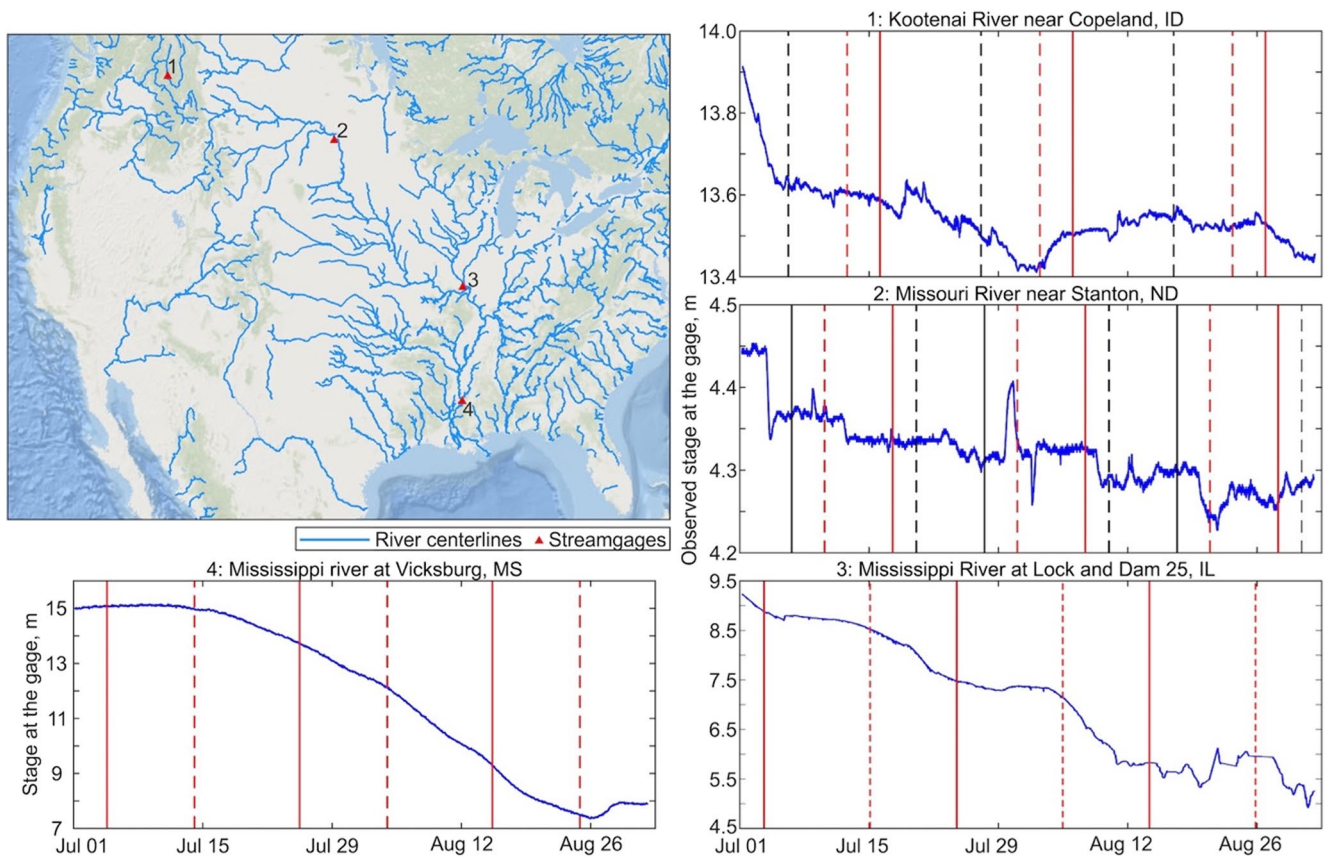


**Figure 4.** Illustration of Surface Water and Ocean Topography (SWOT) temporal sampling at four arbitrary gages (see panels 1–4) in the United States (see map for gage locations), adapted from Frasson (2021). The vertical lines indicate SWOT overpass timing, where each pass is represented by a different line style. The timing of each pass assumes an arbitrary mission start day of January 1 chosen for illustration purposes.

produced and is expected to be of good quality for all rivers greater than 100 m. The ability to produce discharge for rivers as narrow as 50 m will be explored by the SWOT Science Team during the mission.

### 3.2.2. Temporal Characteristics

SWOT will measure most mid-latitude reaches twice on average during the 21 days repeat cycle of the science orbit (~35 observations per year), with more observations at higher latitudes. Figure 3b shows the total number of expected observations per year, after including the effect of ice cover (SWOT discharge will not be estimated when rivers are ice covered). A total of 1,360 river that reaches wider than 100 m (2% of the total) are never observed due to small gaps in SWOT coverage. The effect of ice cover is seen in that the expected number of observations increases with latitude, but then begins to decrease at the highest latitudes; this effect is especially visible in Asia. Figure 4 illustrates SWOT temporal sampling for four United States Geologic Survey gages in North America.

SWOT discharge is included in both the “single pass” data product, defined as the discharge observed at the time of each overpass, and a “cycle averaged” data product. Cycle averaged discharge will be computed as a simple average of all the single-pass discharge estimates for each cycle. For example, if there are three discharge estimates in the 21-day cycle, the cycle-average is the simple mean of the three values.

### 3.2.3. Measurement Precision

SWOT discharge accuracy is impacted by the SWOT WSE, width, and slope measurement accuracy. SWOT science requirements specify that WSE, width, and slope will be computed on all reaches with average width greater than 100 m to reach-scale accuracies of 10 cm, 15%, and 17 mm/km, respectively (JPL Internal Document, 2018). Current estimates of these accuracies differ slightly from the requirements: for example, nominal width accuracy is expected to be on the order of 10 m (Frasson et al., 2017). It may seem surprising that SWOT



can achieve such high precision for width, given that SWOT pixel spatial size varies from 10 to 60 m, in the cross-track direction (Fjørtoft et al., 2014). Note that many such pixels are averaged together to compute river width for a 10 km reach. Figure 5 from Frasson et al. (2021), for example, shows width uncertainties for river nodes (spaced at 200 m downstream) from SWOT radar simulations. Averaging many pixels together leads to width errors on the order of 25 m at the node level. Averaging across ~50 nodes at the reach level will further improve accuracy. Thus, reach-scale width errors are expected to be on the order of 10 m, due to averaging many radar pixels together. We consider  $A'$  to be measured, as it is more-or-less directly estimated from the SWOT measurements of WSE and width; uncertainty in  $A'$  can be approximated to be the product of WSE precision and the river width scaled by  $\sqrt{2}$ , as shown in Appendix A. The effects of WSE, width, and slope uncertainty on SWOT discharge uncertainty is described in Section 5.

### 3.3. Additional Data Sets and the SWORD of Science

In addition to SWORD and SWOT data, other external data sets will also be leveraged to create SWOT data. Specifically, in situ discharge data and modeled discharge estimates will be used in various parts of the discharge creation process. The constrained branch of SWOT discharge will leverage gage data—both historical and concurrent with the SWOT mission; some of the concurrent gage data will be held out for discharge product validation. Details of these data sets are not provided here, but all available gage data will be leveraged.

A priori information for FLPE will be derived from historical global hydrological model simulations. Prior estimates of flow statistics for the unconstrained branch will come from the WBM data set of Cohen et al. (2014). Note that this WBM simulation was not calibrated using gage discharge data and is thus philosophically consistent with unconstrained branch. Prior estimates for the gage-constrained branch will come from GRADES, the Global Reach-Level A Priori Discharge Estimates for SWOT (Lin et al., 2019), a hydrologic model calibrated to in situ gages, and further bias-corrected by gages. Note that the gage constraints in GRADES are not the result of traditional model calibration, that is, GRADES did not use gage time series data to calibrate model parameters, but instead used only global runoff statistics regionalized from several thousand small and naturalized catchments using a neural network (Beck et al., 2015) to constrain the model, which was then run at 2.9 million locations. As a result, the gage constraints in GRADES should be considered indirect and limited, because the runoff percentiles were regionalized from small catchments (10–10,000 km<sup>2</sup>) that mostly fall below the SWOT observable river width limit (50–100 m). A number of additional data sets will be used as prior information in the FLPE process; these are collectively referred to as the “SWORD of Science” (SoS). The SoS combines all additional databases needed for FLPE; some additional details of such data sets are described below.

## 4. How Will SWOT Discharge Be Produced?

SWOT discharge is created by a partnership between the Agencies and Science Team. “Confluence” is the Science Team computational framework for FLPE (Section 4.1), encoding flow laws (Section 4.2), and FLPE methods (Section 4.3). The Agencies produce discharge as part of SWOT data products (Section 4.4). We also present a timeline for SWOT discharge production (see Section 4.5), a plan for discharge evaluation (Section 4.6), and possible Science Team discharge estimates (Section 4.7).

### 4.1. Confluence: A Computational Engine for SWOT Discharge and FLPE

The Confluence computational software engine (<https://github.com/swot-confluence/>) has been developed to enable FLPE in a timely manner from SWOT observations for multiple flow laws across global reaches. All Confluence code is currently publicly available, save for individual Mass-Conserved Flow Law Inversion (McFLI) algorithms which are maintained and made public by their original authors. To support the Agency discharge products, the Science Team will be required to produce FLP estimates rapidly at the global scale. This means we must ingest SWOT observations, reference many data fields within the SWORD database, and run computationally expensive discharge algorithms for on the order of 10<sup>5</sup> reaches, all on a short timeline. This is far from trivial, both in terms of logistics and in terms of the required computational resources. Confluence is a cloud-based computation engine that facilitates these operations; Confluence produces both discharge (to be available as a Science Team data product) and FLP estimates from multiple FLPE algorithms in parallel. Confluence is scalable on demand, both in terms of computational resources and storage

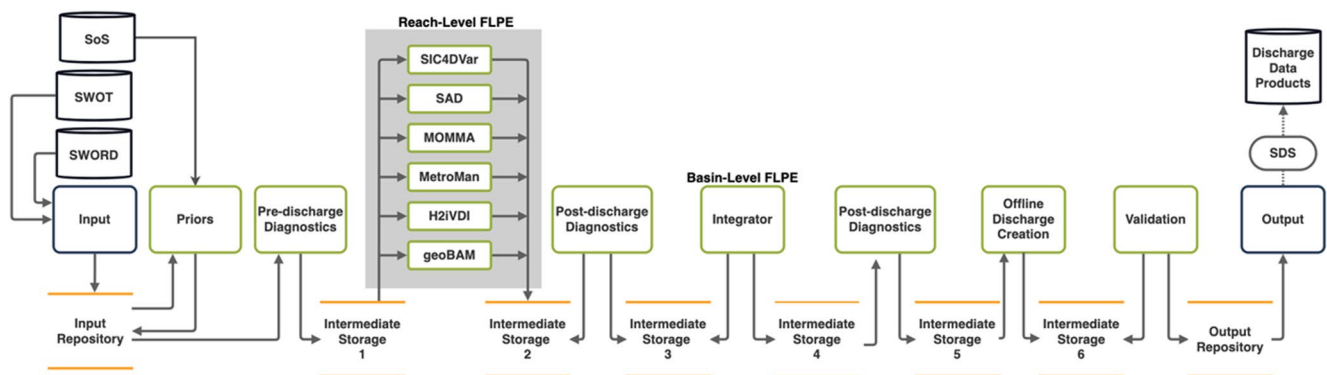


**Figure 5.** Flow law parameter estimation (FLPE) flowchart, in the Confluence software environment. Many of the acronyms and terms are defined in the following subsections. The FLPE algorithms are labeled by whether they operate at the scale of reaches or river basins: see Section 4.3 for more details.

capacity: it is deployable on Amazon Web Services and similar cloud environments with massive computational resources, shortening needed computation time. Optimal FLP estimates produced by Confluence will be merged into SWORD and passed to the agencies to use with discharge production (i.e., step 2, in Figure 2). Confluence includes input modules to interface to all three major data sets described in Section 3.3: SWOT, SWORD, and the SoS. The Confluence inputs and outputs are shown as a flowchart in Figure 5. The algorithms inside Confluence each calculate discharge as well as FLPs, but discharge values computed in Confluence are not passed to the Agencies, but are planned to be available to the community as so-called “Science Team discharge products” (Figure 5; Section 4.7). Confluence is running now on Amazon Web Service (AWS), and has been fully interfaced to read in SWOT data files, and produce the needed FLPs; example Confluence results are presented in Section 4.4. While we anticipate that algorithms will continue to evolve during the mission in order to refine future SWOT discharge, the results shown below demonstrate working software that is currently ready to process SWOT data as described in this paper. All Confluence processing code will eventually be made public. SWOT discharge products will be available approximately 1 year after launch.

#### 4.2. Flow Laws

Flow laws are the functional form that relate SWOT observations of WSE, width, and slope, and FLP estimates to river discharge: see Appendix A. The modified Manning’s flow law shown in Equation 1 is presented as an example flow law. Equation 1 assumes that the nonlinear dynamics of open channel flow in natural rivers can be parameterized via the resistance coefficient ( $n$ , sometimes referred to as the “friction coefficient,” or “Manning’s  $n$ ”) with different possible parameterization models, as described by Rodriguez et al. (2020), Larnier et al. (2020), or Bjerklie et al. (2005). As noted by Ferguson (2010), the resistance coefficient is rarely a constant with river stage. Thus, some flow laws specify  $n_t$  to vary as a function of WSE, while others specify it to vary as a function of  $A'$ , and still others specify it to be a constant. In all these options, these parameters are still functions of space, and therefore possibly different for each node or reach. We describe one example resistance parameterization, for illustration purposes. Following Rodriguez et al. (2020), the resistance coefficient  $n_t$  could take this form:

$$n_t = n_b \left( 1 + \frac{5}{6} \left[ \frac{W_t \sigma_z}{\bar{A} + A'_t} \right]^2 \right), \quad (2)$$

where  $n_b$  is the resistance coefficient at a high flow, such as bankfull, and  $\sigma_z$  is the within-reach spatial variation of river bed elevation. As shown by Rodriguez et al. (2020), the terms in parentheses on the right-hand side of Equation 2 describe the effect of spatial variability within the reach, and  $n_b$  describes any and all forms of energy and momentum loss in the channel including irregular channel geometry, flow irregularities, bedload transport, turbulent lateral and vertical motion in the flow field, form drag around large obstacles (e.g., boulders and fallen trees on the channel bottom) as well as viscous friction losses (Gualtieri et al., 2018). Given this formulation for  $n_t$ , in combination with Equation 1,  $\bar{A}$ ,  $n_b$ , and  $\sigma_z$  denote time-invariant parameters that must be estimated for each reach, using methods described in the next section. While each algorithm will apply a slightly different version of both the flow law and the resistance coefficient formulation, Equations 1 and 2 are representative examples.

Despite the simplicity of this flow law, it has proven remarkably resilient when applied to large rivers across a range of spatial scales, and including special cases such as multiple channels (Altenau et al., 2019), river reaches impacted by low-head dams (Tuozzolo, Langhorst, et al., 2019), and river floodplain interactions (Durand et al., 2014). Reaches with low river slopes (Durand et al., 2020) can be handled simply by relating WSE and river width to river discharge, that is, using a flow law that does not depend on river slope; the FLPs would still be estimated as described below.

### 4.3. FLP Estimation Algorithms

As outlined in Section 2, FLPE is the first step of the two-step process to estimate river discharge using SWOT measurements (see Figure 2). The time-invariant parameters described earlier ( $\bar{A}$ ,  $n_b$ , and  $\sigma_z$  for Equations 1 and 2, as an example) must be estimated for each reach, globally, and for each flow law. Gleason and Durand (2020) describe several approaches to this problem. Here, we present an overview of FLPE methods planned for SWOT discharge (Figure 6). Here, we distinguish between FLPE algorithms that operate at the scale of river reaches (Sections 4.3.1 and 4.3.2) and those that operate at the scale of river basins (Section 4.3.3); these algorithms are listed in Table 1, and briefly described below. Note that a full description of these methods, including their needed inputs and prior information, is outside the scope of this manuscript; for more details on the reach-scale algorithms, see Frasson et al. (2021). All of these algorithms described in this section will be run during the mission, using the Confluence software (Section 4.1).

#### 4.3.1. Reach-Scale Calibration Algorithms

The Modified Optimized Manning Method Algorithm (MOMMA) is a reach scale calibration algorithm and follows the same procedure as typical rating curve calibration (Turnipseed & Sauer, 2010). MOMMA estimates FLPs based on specifying a target discharge estimate. MOMMA is a revised version of the Mean Flow and Geomorphology algorithm (MFG) described by Bonnema et al. (2016) and Durand et al. (2016). MOMMA uses a slightly different version of the modified Manning's equation as Equation 1, and is based on the estimation of bankfull WSE based on analyzing the WSE-width relationship for each reach. MOMMA uses an estimate of bankfull discharge to calibrate the bankfull Manning flow resistance, which is then scaled as a function of relative depth in the channel (equations 1 and 15 in Bjerklie et al., 2018). Bankfull discharge measurements are derived from hydrological model output where in situ discharge is not available. Alternatively, the MOMMA FLPs can be estimated a priori from comparative or statistical information. The accuracy of SWOT discharge estimated via MOMMA is by construction limited to the accuracy of the data used to calibrate, which may include a range of discharge measurements made in the reach or an estimate of the mean discharge for the reach derived from another source.

#### 4.3.2. Reach-Scale Inverse Algorithms

Reach-scale inverse algorithms are designed for use in ungaged basins in areas where there is no in situ data to calibrate against, and where existing estimates of discharge may be poor. These algorithms solve a poorly constrained inverse problem; they incorporate existing estimates of discharge using Bayesian principles, modeling the uncertainty of SWOT observations, flow laws, and prior discharge as part of the inverse algorithm. Tuozzolo, Lind, et al. (2019) and Frasson et al. (2021) showed that such algorithms improve on prior discharge estimates, but that final discharge accuracy is nonetheless dependent to some extent on the prior. Indeed, Larnier et al. (2020) demonstrated that the inversion is ill-posed if based on the flow equations alone; prior information is necessary. Significant effort has been devoted to FLPE inverse algorithms in the SWOT context over the past decade or so (Durand et al., 2010, 2014, 2016; Garambois & Monnier, 2015; Gleason & Smith, 2014; Gleason et al., 2014; Hagemann et al., 2017; Larnier et al., 2020; Nickles et al., 2020; Oubanas et al., 2018; Tuozzolo, Langhorst, et al., 2019; Yoon et al., 2016). The key difference between these and the calibration approach described in the previous section is that these algorithms are designed to solve an under-constrained inverse problem, whereas the calibration approach is well-constrained.

The inverse algorithms described in this section are designed to run on one of two spatial domains: either a single reach, or a set of several reaches. The algorithms that run on a set of several reaches (called an "Inversion Set" here) estimate reach averaged discharge and FLPs for each reach in the Inversion Set, using only reach averaged SWOT observations. Inversion Sets are chosen to minimize lateral inflows, while including as many reaches as possible. Other algorithms operate on a spatial domain of a single reach and estimate discharge and FLPs at each node within

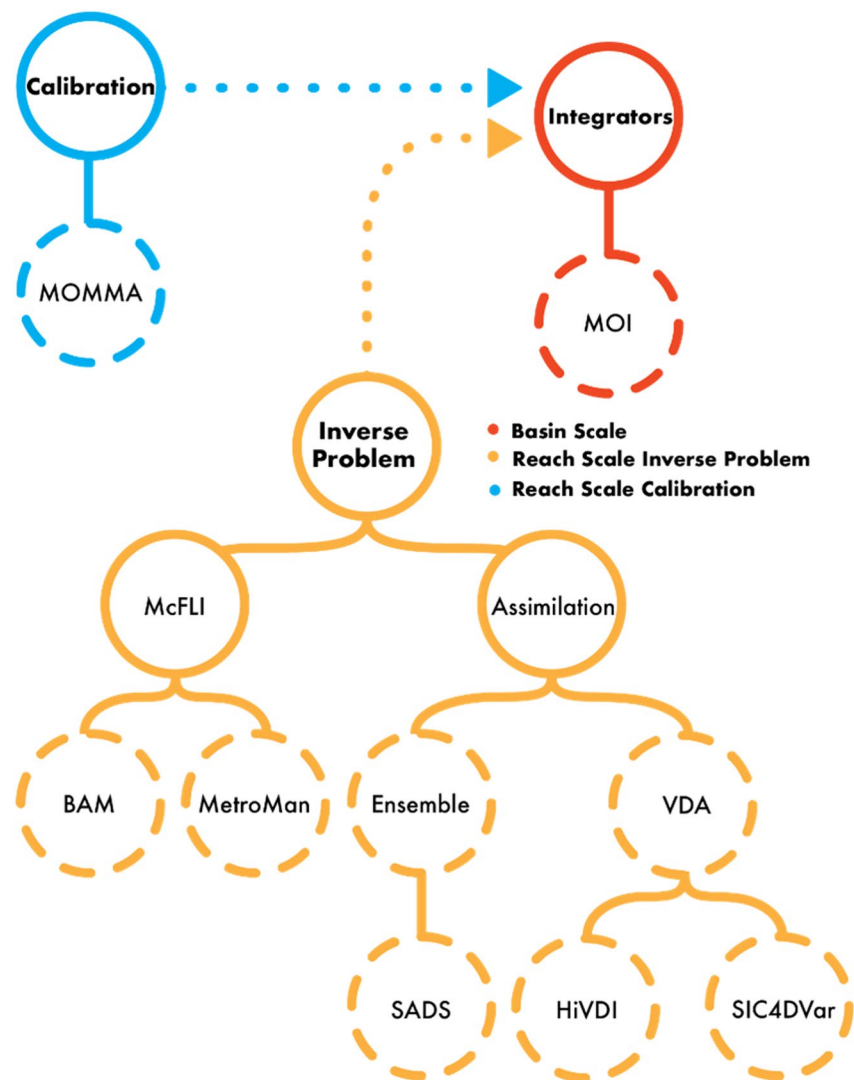


**Figure 6.** Conceptual tree diagram showing the hierarchy of flow law parameter estimation (FLPE) algorithms that make up the first of the two-step process (see Section 2) to estimate Surface Water and Ocean Topography (SWOT) discharge. Circles with solid lines denote the classes of algorithms described in the manuscript, whereas circles with dashed lines denote individual FLPE algorithms. Reach-scale calibration algorithms, reach-scale inverse algorithms, and basin-scale algorithms are shown in blue, yellow, and red, and described in Sections 4.3.1, 4.3.2, and 4.3.3, respectively. Conceptual links in the tree diagram are shown with solid lines, whereas mechanical links are shown with dashed lines: output from the reach scale FLPEs (shown in yellow) is fed into the basin-scale FLPE (shown in red). All acronyms are defined in the text below or in the “Acronyms” at the end of the manuscript.

the reach using SWOT observations at the node scale. Output from inverse algorithms applied at the node scale is averaged to apply to reach scale quantities, in order to interface with the Agency reach-scale discharge estimates.

The algorithms often implicitly or explicitly invoke some form of the continuity equation applied to the spatial domain over which they are applied. They thus neglect tributary inflows and groundwater exchange, making the assumption that such lateral inflows lead to minimal discrepancy between upstream and downstream of the spatial domain. This assumption is obviously more secure when inverting over a single reach at the node scale, but with a tradeoff that SWOT observations are much more uncertain at the node scale than the reach scale: as there are ~50 nodes per reach, node level errors will be on the order of seven times larger. In general continuity-related errors are expected to be minimal across sets of reaches when lateral inflows change the discharge by less than 5% (Nickles et al., 2020).

**Table 1**  
*List of the 14 Discharge Data Values to Be Produced for Each Surface Water and Ocean Topography (SWOT) Pass*

Branch	Prior discharge estimates	FLPE algorithm	Integrator
Unconstrained	WBM	BAM	MOI
Unconstrained	WBM	HiVDI	MOI
Unconstrained	WBM	MetroMan	MOI
Unconstrained	WBM	MOMMA	MOI
Unconstrained	WBM	SAD	MOI
Unconstrained	WBM	SIC4DVar	MOI
Unconstrained	WBM	Consensus	–
Gage-constrained	GRADES	BAM	MOI
Gage-constrained	GRADES	HiVDI	MOI
Gage-constrained	GRADES	MetroMan	MOI
Gage-constrained	GRADES	MOMMA	MOI
Gage-constrained	GRADES	SAD	MOI
Gage-constrained	GRADES	SIC4DVar	MOI
Gage-constrained	GRADES	Consensus	–

*Note.* The source of the prior on historical river discharge statistics is also provided; note that other a priori information required for each algorithm is not detailed here. FLPE is flow law parameter estimation. All acronyms are defined in the text or in the “Acronyms” at the end of the manuscript.

There are multiple classes of algorithms proposed to be used, including McFLI and variational data assimilation (VDA) as shown in Figure 6 and described in the next two subsections.

#### 4.3.2.1. Mass-Conserved Flow Law Inversion

McFLI refers to inverse algorithms that infer FLPs by equating discharge in neighboring adjacent reaches or nodes of the river, over a specified spatial domain (Gleason et al., 2017). McFLI algorithms thus invoke flow laws (Manning’s equation or hydraulic geometry) and continuity (conservation of mass among neighboring nodes or reaches). Two McFLI algorithms are currently planned for use with SWOT.

The geomorphically informed Bayesian “At-many-stations” hydraulic geometry-Manning Algorithm (geoBAM; Brinkerhoff et al., 2020) leverages the concept of “At-many-stations” hydraulic geometry (AMHG; Gleason & Smith, 2014) to jointly invert Equation 1 and traditional hydraulic geometry as expressed by Brinkerhoff et al. (2019) following Dingman (2007). This flow law has been simplified since geoBAM’s original publication to remove redundant parameters and use only the primal terms of hydraulic geometry per Dingman (2007): bankfull width, bankfull depth, channel shape parameter  $r$ , and Manning’s  $n$ . geoBAM builds from the original BAM algorithm of Hagemann et al. (2017) by introducing additional prior information. geoBAM assumes steady flow within each reach and is fully Bayesian: it models the uncertainty on each input including the observations and prior estimates of discharge and the FLPs to produce explicit posteriors on all terms in Equation 1. geoBAM first classifies rivers in SWOT according to their geomorphology, and then assigns priors according to geomorphology and discharge prior information.

The Metropolis-Manning (MetroMan) algorithm (Durand et al., 2014) is conceptually similar to geoBAM, and thus we highlight only the most important differences. MetroMan uses only the Manning’s equation flow law as

written in Equation 1. MetroMan for SWOT will be applied to reaches, whereas geoBAM will be applied to nodes. MetroMan applies a continuity equation to adjacent reaches such that the difference in flow between adjacent reaches is equated to the change in storage within the reaches; thus, steady flow among reaches is not assumed as it is for geoBAM. The MetroMan mass balance equation will revert to steady flow when the time-resolution of SWOT is inadequate to resolve floodwave dynamics for a particular river. MetroMan will use a subset of the prior information used by geoBAM.

#### 4.3.2.2. Data Assimilation

Data assimilation (DA) approaches differ from McFLI in that they invoke a calibration process and/or a parameter identification process using a hydraulic model. The hydraulic model could be dynamic (e.g., the shallow water equations) or steady (e.g., the gradually varied flow equation), but in both cases the model requires river discharge and cross-section geometry as inputs, and computes WSE and river width as outputs. DA with hydraulic models requires a prior estimate of FLPs (bathymetry, friction) and discharge, which are then optimized by minimizing the difference between the model outputs and the observations. For SWOT discharge, DA algorithms provide FLP values based on the assimilation output.

VDA algorithms in this context invoke a 1-D dynamic hydraulic model and its adjoint counterpart. They allow the assimilation of available SWOT observations within an assimilation window (i.e., a subset of the available observation times) through a forward and a backward run of the model at each minimization step. The observed hydraulic dynamics are propagated in both space and time. They provide an estimate of the model inputs/variables (posterior estimate) over the entire window (Oubanas et al., 2018).

Two VDA algorithms are under development for use with SWOT observations. The Hierarchical Variational Discharge Inference (HiVDI) algorithm is based on a hierarchical McFLI—VDA method; it is planned to run globally (Larnier et al., 2020). The McFLI-based modules in HiVDI enable the production of consistent prior

estimates, as well as final FLP and corresponding estimates. The VDA module, based on the Saint-Venant equations, estimates discharge in both space and time, along with the bathymetry and a time-varying friction coefficient. The VDA module takes node-scale inputs, and creates node-scale FLP outputs. The final reach-scale FLP estimates are computed from the node-scale results. This algorithm and the related DassFlow software are open source (<http://www.math.univ-toulouse.fr/DassFlow/>).

A simplified version of the SIC4Dvar algorithm described by Oubanas et al. (2018) will also be deployed at the global scale. In this version, a steady flow model will be configured and deployed for SWOT reaches instead of the full unsteady flow model. A Bayesian analysis is performed, weighing the prior information on average flow statistics with the likelihood function based on the difference between modeled and measured WSE, width, and slope. FLPs will then be estimated by minimizing the difference between the discharge outputs obtained from the Bayesian analysis and the modified Manning equation applied to the SWOT observations.

The SWOT Assimilated Discharge (SAD) algorithm (Andreadis et al., 2020) differs significantly from the VDA algorithms. SAD is best thought of as a batch ensemble Kalman smoother. An ensemble of FLPs at the node scale is created from prior information. The prior FLPs are used to create an ensemble of river discharge estimates, for each pass, assuming steady flow. Then the steady gradually varied flow equation is solved for the prior ensemble, predicting river WSE and width at each node for each member of the ensemble. The differences between SWOT measurements and prior predictions are used in the Kalman analysis to compute a posterior estimate of both discharge and FLPs.

#### 4.3.3. Basin-Scale Integrator Algorithms

The reach-scale algorithms (Sections 4.3.1 and 4.3.2) are designed to run on a limited spatial domain. Applying the inverse algorithms described above across an entire river network in a single computational analysis is currently computationally infeasible, necessitating that a large river network be handled either one reach at a time, or one Inversion Set at a time. Thus, a second class of algorithms is being developed that will “integrate” reach-scale algorithm results across river networks. Integrators will ensure that flow is conserved at river confluences. These algorithms are designed to run at basin scale, and to be used for both the gage-constrained and the unconstrained discharge estimates. In addition to leveraging flow conservation across river networks, integrators will combine reach-scale algorithm results with in situ data for the gage-constrained products.

The Mean Optimization Integrator (MOI, unpublished; see Section 5, e.g., results) is designed to run over a time series of SWOT observations once discharge has been computed. First, MOI estimates mean flow for each river in the network. This estimate can be computed mathematically as a linear problem by enforcing flow conservation at river junctions and throughout the river network and solving for the estimates of river discharge that are closest to the estimates derived from the inverse and calibration algorithms. For gage-constrained discharge, MOI will add in situ gages to the optimization objective function with a far lower uncertainty than specified for the FLPE estimates where gages are not available. This is a straightforward constrained optimization problem and can be solved with widely available computational solvers. Outliers from the reach-scale algorithms will be identified by running MOI iteratively. Second, MOI computes discharge uncertainty via an ensemble approach. An ensemble of mean flow is computed from reach-scale estimates of discharge uncertainty, and the optimization problem is solved for each ensemble member. The final uncertainty is computed from the standard deviation across the ensemble of optimal mean flow estimates. Third, the optimized mean flow estimates are used to infer optimal FLPs. Integrators would be applied to both the gage-constrained and unconstrained discharge estimates. MOI will account for inflow from rivers not observed by SWOT, channel withdrawals, and gain or loss of discharge from hyporheic exchange from globally available data sets by modifying the optimization constraints. For example, contribution of discharge from rivers not observed by SWOT will be estimated from models used for global prior estimates of mean flow.

MOI will also be run across river networks that include storage features such as lakes and reservoirs. Invoking mass balance between the rivers and lakes, the difference between flow into and out of lakes is equal to the change in lake storage, and evaporation from the lake surface (assuming limited groundwater exchange). As suggested by Wang et al. (2021), Xin. (2022), and Riggs et al. (2022) SWOT measurements of lake volume variation can largely capture this discharge-storage interaction, and be used as another constraint on river discharge. Lake evaporation estimates derived following Zhao and Gao (2019) will thus be combined with SWOT lake storage change measurements to improve the estimates of FLPs.

MOI constrains mean flow to be conserved across the SWOT-observed river network but does not enforce physical constraints on the time-varying SWOT discharge data. Although they were not in place before SWOT launch, future integrators could include global scale hydraulic models and DA such as the approach of Ishitsuka et al. (2021).

#### 4.3.4. FLPE for the Gage-Constrained Discharge Estimates

FLPE is performed similarly for the gage-constrained and unconstrained discharge estimates. For the reach-scale algorithms, unconstrained FLPE uses priors from WBM, a model which was not calibrated to in situ gages. Gage-constrained FLPE uses priors from GRADES, which did use in situ gages; furthermore, gages are applied directly as priors for reach-scale algorithms, where available. For the basin-scale, no gages are used for MOI FLPE for the unconstrained products. For the gage-constrained products, MOI applies gaged mean flow directly to the analysis wherever gages are available. The constrained discharge will leverage both real-time and historical data. Historical gage data will be leveraged by creating relationships between satellite measurements from other remote platforms (e.g., river width derived from Landsat) and historical discharge data. This will allow discharge prediction concurrent with SWOT observations, which can then be used for both reach-scale and basin-scale FLPE for the gage-constrained product.

#### 4.4. Example Discharge Estimates and Data Products

Example FLP estimates are shown in Tables 2 and 3 and example Agency discharge estimates are shown in Figure 7. These estimates were produced by an end-to-end simulation, beginning with SWOT reach-scale measurements of height, width, and slope, computing FLPs, and final SWOT discharge estimates, as they would be distributed by the space agencies. These estimates are informed by calibration to mean annual flow from hydrologic models, or constrained using gage information just as they will be during the mission. SWOT measurements were synthesized by mimicking SWOT space-time sampling and expected error distribution. The true height, width, and slope values were created using the Ohio River Community HEC-RAS Model (Adams et al., 2018). Model outputs were sampled at the times of SWOT orbits, errors were added to the data using the methods of Frasson et al. (2021), to create files that closely resemble the SWOT Level 2 single pass data format (JPL Internal Document, 2020). These synthesized data products were ingested into Confluence as shown in Figure 5. Tables 2 and 3 show the reach-scale and basin-scale FLP estimates. The discharge values shown in Figure 7 are an almost exact replica of the software to be used by the agencies to create Agency discharge estimates (Coss et al., 2022).

Several important aspects of SWOT discharge are illustrated in these example discharge estimates. First, as described in Section 2, the science team will create FLP estimates and provide these to the space agencies: these FLP estimates are shown in Tables 2 and 3. The agencies will use these FLP estimates to create Agency SWOT discharge, shown in Figure 7. Second, SWOT discharge will contain both a gage-constrained and an unconstrained branch of FLP and discharge estimates, for example, Tables 2 and 3 represent the FLP estimates for the gage-constrained and unconstrained products, respectively. Third, for each branch, SWOT discharge will include a small ensemble of discharge estimates, computed using the various FLPEs described in the previous section. These are shown as separate time series in Figure 7, and separate sections of Tables 2 and 3. Fourth, the “consensus” discharge will be computed in the second of the two-step process for computing river discharge, computed as an average across the ensemble of discharge estimates estimated from the six other algorithms, weighted by their respective uncertainties. Thus, the discharge data elements listed in Table 1 will be produced for each reach and each pass: seven for the unconstrained branch, and seven for the constrained branch.

#### 4.5. FLPE and Discharge Production Timeline

SWOT measurements of river WSE, width, and slope will be available during the mission, Agency-produced discharge will be available after the Science Team has computed FLP estimates and provided them to the space agencies, and will be available with the same latency as the rest of the level 2 data products such as river WSE, width, and slope. For optimal results, FLPE must be performed over periods with significant changes in river flows. As many seasonal rivers vary little in the dry season, the Science Team expects to deliver the first estimate of FLPs to the Agencies after performing FLPE analyses on approximately 1 year of data. The so-called “validation meeting” (a key mission landmark) is expected to take place 8 months after transitioning to the nominal science orbit (see Section 3.2). The SWOT Science Requirements Document specifies that Agency discharge estimates will begin to be produced not later than 6 months after the validation meeting; as launch took place in December 2022, Agency discharge estimates are planned to be available in August 2024. Note that other SWOT measurements, such as river WSE, width, and slope, are planned to be made public much earlier. Following the

**Table 2**

*Example Flow Law Parameter Estimates for Seven Reaches on the Mississippi River for the Gage-Constrained Branch of the Surface Water and Ocean Topography (SWOT) Discharge Estimates*

MetroMan	Reach-scale flow law parameters			Basin-scale flow law parameters		
	Abar	Ninf	<i>b</i>	Abar	ninf	<i>b</i>
Reach #						
74270100211	10,848.53	0.03	1.04	9,045.63	392.21	−4.76
74270100221	10,548.05	0.03	1.50	10,556.17	37.07	−3.25
74270100231	11,107.28	0.03	1.75	8,832.68	3,759.82	−5.48
74270100191	11,073.69	0.03	0.92	11,112.76	0.43	−0.89
74270100171	11,298.95	0.03	1.06	11,333.25	1.62	−1.54
74270100151	9,027.99	0.03	0.64	9,043.53	0.070	0.14
74270100131	11,305.57	0.03	1.61	10,434.40	3,741.31	−4.97
BAM	Db	<i>n</i>	<i>r</i>	A0	<i>n</i>	−
Reach #						
74270100211	8.33	0.02	5.07	4,617.83	0.01	−
74270100221	−	−	−	5,520.33	0.01	−
74270100231	−	−	−	4,995.10	0.07	−
74270100191	7.58	0.02	5.06	11,014.53	0.04	−
74270100171	9.25	0.02	5.48	9,002.57	0.10	−
74270100151	−	−	−	9,173.97	0.03	−
74270100131	−	−	−	8,349.20	0.01	−
HiVDI	Abar	alpha	beta	Abar	alpha	beta
Reach #						
74270100211	2,774.84	85.35	−0.05	2,825.41	679.80	−0.84
74270100221	4,199.46	47.46	−0.05	4,203.96	205.73	−0.38
74270100231	2,916.82	85.03	−0.05	2,949.35	568.34	−0.79
74270100191	754.88	56.04	−0.05	3,330.44	322.62	−1.29
74270100171	1,627.21	69.67	−0.05	3,096.04	459.58	−1.14
74270100151	5,426.60	35.97	−0.05	5,749.18	56.13	−0.62
74270100131	1,800.34	91.61	−0.04	2,515.77	831.40	−1.35
MOMMA	<i>B</i>	<i>H</i>	−	<i>B</i>	<i>H</i>	−
Reach #						
74270100211	49.860	83.73	−	73	90.55	−
74270100221	39.94	84.23	−	74.73	91.23	−
74270100231	62.65	85.62	−	73.96	81.25	−
74270100191	71.68	89.77	−	77.40	92.48	−
74270100171	67.22	86.72	−	73.97	91.49	−
74270100151	73.54	85.86	−	69.18	439,900.06	−
74270100131	62.60	84.89	−	71.13	90.18	−

initial release of the Agency discharge estimates, discharge estimates will be available in near-real time following each satellite overpass. It is our hope to update FLPs 1–2 times per month. As the length of time to perform FLPE grows with the mission lifetime, the FLPEs are expected to become more accurate and more precise; thus, FLPs for the Agency discharge product expected to be updated multiple times throughout the mission lifetime.



**Table 3**

As Table 2, Except for the Unconstrained Branch of Surface Water and Ocean Topography (SWOT) Discharge Estimates

MetroMan	Reach-scale flow law parameters			Basin-scale flow law parameters		
	Abar	ninf	<i>b</i>	Abar	ninf	<i>b</i>
Reach #						
74270100211	9,911.04	0.03	0.68	10,027.03	0.43	−1.26
74270100221	9,331.77	0.03	0.59	9,462.11	0.13	−0.80
74270100231	9,836.49	0.03	0.71	9,723.08	0.74	−1.45
74270100191	10,195.97	0.03	0.53	10,152.67	0.01	1.07
74270100171	10,480.92	0.03	0.61	10,499.63	0.02	0.35
74270100151	9,415.54	0.04	0.37	9,345.89	0.01	1.25
74270100131	10,460.51	0.03	0.81	10,435.34	0	1.50
BAM	Db	<i>n</i>	<i>r</i>	A0	<i>n</i>	−
Reach #						
74270100211	8.04	0.02	4.68	2,737.13	0	−
74270100221	7.45	0.02	5.72	3,056.28	0	−
74270100231	5.61	0.02	3.77	2,229.71	0	−
74270100191	7.06	0.02	5.26	3,310.92	0.01	−
74270100171	6.40	0.02	5.61	3,082.77	0.01	−
74270100151	−	−	−	3,190.92	0.02	−
74270100131	−	−	−	2,476.79	0	−
HiVDI	Abar	alpha	beta	Abar	alpha	beta
Reach #						
74270100211	1,228.19	49.02	−0.05	2,742.23	234.04	−0.03
74270100221	1,380.80	51.51	−0.050	3,065.90	289.13	0
74270100231	5,372.95	21.78	−0.05	5,372.53	0.07	4.11
74270100191	5,095.86	51.71	−0.05	4,818.42	30.48	0.15
74270100171	485.28	62.22	−0.05	3,085.41	180.23	−0.36
74270100151	3,890.62	35.59	−0.05	3,849.21	23.61	0.12
74270100131	1,800.34	36.08	−0.05	2,578.97	298.13	−0.53
MOMMA	<i>B</i>	<i>H</i>	−	<i>B</i>	<i>H</i>	−
Reach #						
74270100211	72.25	85.61	−	75.94	85.33	−
74270100221	36.32	86.73	−	76.24	91.23	−
74270100231	68.10	85.90	−	75.34	91.79	−
74270100191	71.68	89.77	−	78.67	81.78	−
74270100171	67.22	86.72	−	75.65	89.49	−
74270100151	73.54	85.86	−	76.77	156.37	−
74270100131	61.74	85.58	−	73.55	88.18	−

#### 4.6. Discharge Evaluation

Both the gage-constrained and the unconstrained branches of the SWOT discharge estimates will be validated using in situ discharge data that was not used (and is completely independent of) data used to produce gage-constrained discharge. The purpose of evaluating or validating discharge is to produce reliable discharge

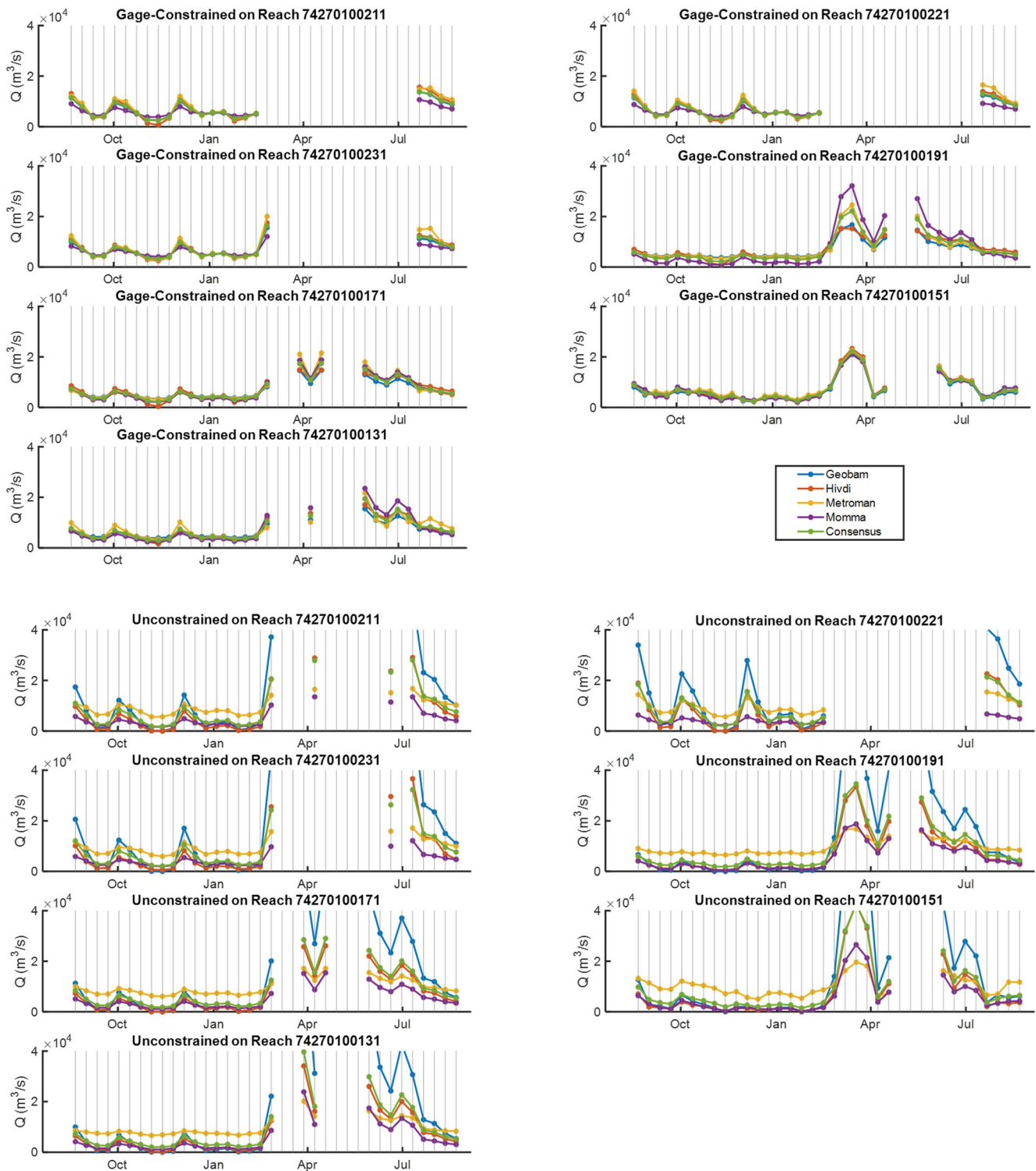


**Figure 7.** Example simulated Surface Water and Ocean Topography (SWOT) discharge ( $Q$ ) results mimicking Agency-led data products for seven reaches on the Mississippi River. Branch (i.e., either gage-constrained or unconstrained) and SWOT mission river database (SWORD) reach IDs are shown in titles of each subplot. The various colored lines indicate each flow law parameter estimation algorithm, and are labeled in the figure legend. Note that some values exceed  $Y$  axis limit.

benchmark values that can be used to approximate global accuracy. We will use discharge data from all available sources to evaluate discharge accuracy, including gages maintained by global agencies, and streamflow measurements available to the science team, including those measured by the SWOT calibration and validation team. We expect that discharge accuracy and uncertainty will vary among rivers, and we will stratify accuracy assessment

across rivers by geomorphic class, river size, and other factors. Discharge evaluation is planned to be complete by the time the Agency product is publicly available.

It is important to note that gage and field discharge measurements are not perfect, even though they are the reference for evaluating SWOT discharge (Coxon et al., 2015; Kiang et al., 2018). Any difference between SWOT discharge and gage discharge necessarily reflects error in both SWOT discharge and in situ discharge.

Each gage will be assigned to be for either FLPE or validation; we will not split the record at each gage into calibration versus validation but will instead assign the entire time-series record for each gage to either calibration or validation. The strategy to split in situ gage data into calibration/training and validation can be thought of as an experiment design problem. The purpose of the experiment design is twofold: First, we require characterization of the performance of all SWOT discharge products, to fulfill the science requirement that: “The SWOT discharge performance shall be quantified by a payload independent measurement or analysis during a post-launch validation period as well as during the mission lifetime.” (JPL Internal Document, 2018). Second, we seek to make the gage-constrained products as accurate as possible, using a subset of available in situ discharge data. Thus, we will split the data into calibration/training and validation sets, with the goal being to make the constrained products as accurate as possible, while saving enough data to fully evaluate SWOT discharge accuracy. In addition to gage data, the SWOT validation team will use ADCPs to collect in situ discharge measurements coincident with SWOT overpasses at select locations during the mission. We expect SWOT discharge accuracy for each reach to vary significantly in time, similar to how accuracy varies at a gage, and thus will break out SWOT discharge evaluation by flow regime.

#### 4.7. Discharge Estimates Beyond the Agency Products

The preceding sections have discussed only Agency discharge estimates that will be provided globally in fulfillment of the SWOT Science Requirements document: that is, river discharge computed by the space Agencies using SWOT observations and FLPs computed by the Science Team. Agency discharge estimates will be available through Agency-funded data distribution centers, with full documentation compliance. However, SWOT measurements of WSE, width, and slope enable a wide range of methods to estimate discharge. The Agency-produced discharge paradigm is somewhat restricting: it requires, for example, that discharge be computed using simple flow laws with parameters estimated offline. One possible example of a science team produced data product would be spatio-temporal interpolation of Agency-produced products (Paiva et al., 2015), or to assimilate the Agency products (Emery et al., 2020). These approaches (and the other options below) could move beyond the need to have a Manning-type formulation of discharge. A second possible product could assimilate the discharge estimates computed in the reach-scale algorithms into a global hydrological model (Ishitsuka et al., 2021). A third approach is to assimilate the SWOT observations of WSE, width, and slope directly into global hydraulic and hydrologic models (Andreadis et al., 2007; Biancamaria et al., 2011; Li et al., 2020; Wongchuig-Correa et al., 2020; Y. Yang et al., 2019). This approach would require global hydraulic models that adequately represent river hydraulic structures, waterfalls, and so on. Now that such data sets are beginning to be available globally, along with global simulations of river hydraulics (Getirana et al., 2017; Yamazaki et al., 2011) and noting the possibility that bathymetry could be refined in real-time by the assimilation (Yoon et al., 2012), such an approach appears increasingly feasible. A fourth possible product could use the Agency products as priors to estimate discharge and bathymetry at finer scales using hydraulic models and DA in order to account for dynamics over a larger area of the river and hence a denser spatial and temporal SWOT coverage (Oubanas et al., 2018). A fifth example could begin to work toward a constellation approach for surface water, similar to the Global Precipitation Mission (Huffman et al., 2020). SWOT measurements would be complemented by measurements of WSE from nadir altimeters, and measurements of river width from visible band imagery and radar. FLPE may rely on SWOT measurements, but once these parameters are estimated, they can be applied to any measurements of WSE and river width. A sixth option would be to reprocess the actual pixel cloud measurements to estimate WSE and river width in each channel in multi-channel river environments, to improve estimates of river discharge in braided and anastomosing rivers. Note that ~10% of river reaches in SWOT are multi-channel rivers. A seventh option is to better estimate river discharge for low slope reaches by bringing more information related to tides in coastal environments. Ultimately, one advantage of Science Team data products is that they can be flexible based on the characteristics of the SWOT during the mission and the creativity of the research community. As such, we expect rapid innovations in these algorithms, some of which may ultimately be incorporated into later versions of the

Agency-led discharge products. Science team-derived discharge data products will be made available publicly after the Science Team has produced and validated these products.

## 5. Expected SWOT Discharge Accuracy

The previous section described how SWOT discharge is computed; this section describes how accurate SWOT is expected to be, which determines its potential scientific applications. Discharge accuracy is the degree to which discharge estimates conform to the true discharge values and is assessed by a range of accuracy measures based on the error at each time  $\epsilon_t$ :

$$\hat{Q}_t = Q_t^* + \epsilon_t \quad (3)$$

where  $\hat{Q}_t$  is the SWOT discharge estimate, and  $Q_t^*$  is the true discharge at SWOT overpass times for a given river reach. Note that  $Q_t^*$  is unknown: the gaged discharge we will use for evaluating SWOT products has its own uncertainty. SWOT discharge errors will have both random and systematic components; for the purpose of this paper, we define systematic errors as those that would produce a discharge time-series bias, and random errors as those that would produce a zero mean  $\epsilon_t$  time series. Uncertainty of a discharge estimate “describes the expected magnitude of the error by characterizing the distribution of error that would be found if the [estimate] was infinitely repeated” (Povey & Grainger, 2015). As both systematic and random errors are important in this context, SWOT discharge will include measures of both random and systematic uncertainty, to be estimated using the process of Uncertainty Quantification (UQ) described by Smith (2013). Uncertainty estimates themselves are subject to evaluation through validation against in situ discharge data: after accounting for gage discharge uncertainties, inaccurate SWOT discharge uncertainty estimates will not correctly describe the magnitude of differences between gaged and SWOT discharge. Considering Equation 1, discharge uncertainty derives from FLPs, SWOT measurements, and the “approximation error” (as defined by Povey and Grainger (2015)) associated with the flow law itself.

Based on algorithm intercomparison studies (Durand et al., 2016; Frasson et al., 2021), SWOT discharge is expected to be dominated by systematic error, manifesting as time-series bias. Systematic errors as we define them arise predominantly because the FLP estimates are constant in time and used in Equation 1 for all discharge computations in a time series (Frasson et al., 2021). The result will be that all discharge estimates in the time series at that reach will be affected in the same way.

We define random and systematic measures of both accuracy and uncertainty. In evaluating the discharge products against field data, the expected magnitude of error  $\epsilon_t$  will be measured by the mean and standard deviation of  $\epsilon_t$ , which we denote as  $b_Q^*$  and  $\sigma_Q^*$ , respectively, where the \* superscript indicates that these measures are assumed to characterize the actual error. The gage uncertainty must also be considered in interpreting values of  $b_Q^*$  and  $\sigma_Q^*$ : though we refer to  $\epsilon_t$  as “error” for simplicity, in interpretation, we must treat  $\epsilon_t$  only as a difference between two uncertain estimates. A range of other accuracy measures will also be used: see Frasson et al. (2021). We propose two measures of uncertainty. The random part of the time-varying discharge time-series uncertainty  $\sigma_{Q_{rand}}$ ; we allow for  $\sigma_{Q_{rand}}$  to vary from pass to pass, and thus we expect uncertainty to capture any seasonal variations in SWOT discharge accuracy, as well as pass-to-pass variations in WSE, width, and slope measurement accuracy. The systematic part of the discharge time-series uncertainty will be defined as  $s_{bQ}$ ; it reflects the uncertainty in the time-series mean of the discharge at a reach. The sum of squared relative and systematic uncertainty is analogous to the relative RMSE metric defined by Bjerklie et al. (2005). The following sections describe how  $\sigma_{Q_{rand}}$  and  $s_{bQ}$  are calculated from the three main sources of uncertainty for SWOT discharge: SWOT observation error, flow law approximation error, and FLP error.

### 5.1. Uncertainty Due To SWOT Observation Error

SWOT observations contribute to the random part of SWOT discharge uncertainty. Discharge uncertainty due to SWOT observations can be represented via first-order Taylor series uncertainty propagation following Yoon et al. (2016). Normalized by discharge,  $\sigma_{Q_{obs}} Q^{-1}$  is the uncertainty in SWOT discharge due to observations, and will be computed as:

$$\left(\frac{\sigma_{Q_{Obs}}}{Q}\right)^2 = \left(\frac{5}{3} \frac{\sigma_{A'}}{\bar{A} + A'}\right)^2 + \left(\frac{2}{3} \frac{\sigma_W}{W}\right)^2 + \left(\frac{1}{2} \frac{\sigma_S}{S}\right)^2 \quad (4)$$

Uncertainty in the SWOT observations is denoted by “ $\sigma$ ” and will be available as part of the SWOT river single pass data product (JPL Internal Document, 2020); see Section 3.2.3 for more details.

### 5.2. Uncertainty Due To Flow Law Approximation Error

Flow law approximation error contributes to the random part of SWOT discharge uncertainty. Using a single flow law to describe the full range of discharge in a river reach assumes that the energy loss at different flow levels can be captured by a continuous mathematical representation of the balance between the energy supplied (the slope) and the energy lost (flow resistance). In fact, the relation between energy gained and lost can be discontinuous and highly variable depending on the level of flow, the shape of the channel (in planform and in cross-section), sediment transport, and the non-uniform distribution of obstacles in the river. To first order, erosion within one part of a reach and deposition within another is not expected to lead to large errors. However, large flow events leading to significant erosion or deposition across the entire reach would change  $\bar{A}$  and would add to uncertainty, but would be expected to happen infrequently within the SWOT mission lifetime.

Many estimates of Manning equation flow law accuracy are provided in the literature, but relatively few exist that meet the criteria that match how SWOT data will be used, using precise, time-varying estimates of river slope (Tuozzolo, Langhorst, et al., 2019). Moreover, most studies do not partition out the part of the validation accuracy due to observation uncertainty (in both discharge and river WSE, width and slope), and due to the flow law itself. Frasson et al. (2021) assessed flow law accuracy across a range of river reaches, and river flows, by comparing the simple flow law formulations described in Section 4.2 applied at the reach scale to hydraulic models that resolve the complete shallow water equations at the cross-section scale, and demonstrated typical flow law accuracy of approximately 5%, for a nominal case when flow is in-bank.

We would expect conditions such as out-of-bank flow to increase the flow law approximation error. Resistance changes dramatically for out-of-bank conditions, such as when flow occurs over vegetation. We note that error in FLP uncertainty tends to dominate over flow law approximation error, even for out-of-bank flow (Durand et al., 2016).

### 5.3. Uncertainty Due To FLP Error

FLP error includes uncertainty due to  $\bar{A}$  as well as the resistance coefficient  $n$ , and its associated parameters. As a tangible example to help visualize FLP error, consider the following thought experiment. Imagine that for a particular reach, McFLI is performed using an ensemble of prior estimates of mean annual flow, derived from different global hydrological models. Consider the posterior set of FLP estimates for each member of the ensemble, along with the bias  $b_Q^*$  of each ensemble member. The standard deviation across the ensemble of mean flow estimates is analogous to  $s_{b_Q}$ . Note that  $s_{b_Q}$  does not indicate the standard deviation of a time series, but rather is a measure of the expected dispersion of the mean flow for that reach due to FLP estimates. The key element of this definition of  $b_Q^*$  is that it includes not just the uncertainty encapsulated in the posterior covariance of the handful of parameters given by a Bayesian McFLI algorithm, but also the uncertainty introduced by errors in the mean annual flow supplied to that McFLI algorithm. At the moment, McFLI algorithms do not account adequately for these error sources, but we want to leave the path open for this to be tackled in future work. The definition of  $s_{b_Q}$  will be re-evaluated during the mission, and will be replaced with the interquartile range or another statistic if it becomes evident that discharge uncertainty in mean flow is highly skewed.

Systematic error in discharge is mostly due to error in FLP estimates but relating  $s_{b_Q}$  to parameter uncertainty is not trivial. For one thing, not all reach-scale algorithms produce explicit estimates of the parameter variances. Thus, in practice,  $s_{b_Q}$  values for each reach-scale algorithm will be specified based on algorithm intercomparison studies such as Durand et al. (2016) and more recently Frasson et al. (2021). Future work will explore mapping between parameters and systematic error. Basin-scale integrators will be applied to reach-scale output, and thus  $s_{b_Q}$  estimates will be refined as a result, as shown in a simple example, in Section 5.5.

#### 5.4. Combined Estimates of Random and Systematic Uncertainty

We here assume that SWOT observations and flow law approximation contribute only to random error, and that parameters contribute only to systematic error in discharge. This is not a perfect assumption in all cases: for example, error in parameter estimates contributes to distortion in the hydrograph, which could impact discharge standard error (Durand et al., 2010). Similarly, because Manning's equation is non-linear, random error in the observations may contribute a change in the mean of the discharge predictions. The assumptions we make here allow us to make a first-order estimate of SWOT discharge uncertainty.

The total random error component can be estimated from the component due to flow law approximation ( $\sigma_{Q_{FLA}}$ ), and to observations ( $\sigma_{Q_{Obs}}$ ):

$$\left(\frac{\sigma_{Q_{rand}}}{Q}\right)^2 = \left(\frac{\sigma_{Q_{Obs}}}{Q}\right)^2 + \left(\frac{\sigma_{Q_{FLA}}}{Q}\right)^2 \quad (5)$$

The total uncertainty  $\sigma_{Q_{tot}}$  is analogous to a relative root mean square error (rRMSE as defined by Bjerklie et al. (2005)), and can be written as the combination of the mean and standard deviation, that is, the random and systematic terms:

$$\left(\frac{\sigma_{Q_{tot}}}{Q}\right)^2 = \left(\frac{\sigma_{Q_{rand}}}{Q}\right)^2 + \left(\frac{s_{bQ}}{Q}\right)^2 \quad (6)$$

The next step is to relate  $\sigma_{Q_{rand}}$  and  $s_{bQ}$  to the three primary sources of discharge error: FLP error, error in SWOT observations, and flow law approximation. In the following sections, we model these quantities and describe the current best estimates of their magnitudes, to better visualize SWOT discharge uncertainty.

#### 5.5. Example Estimates of Uncertainty in SWOT Discharge

We apply the MOI integrator described in Section 4.3.3 to enforce conservation among reaches and incorporate gage discharge where available, to reduce systematic discharge uncertainty. These are presented as sample results only: they will be updated using real SWOT data during the mission. Here, we are leveraging the fact that inverse algorithm results have generally been found to have uncorrelated errors from one river reach to another (Durand et al., 2016; Frasson et al., 2021). In reality, some degree of correlation is to be expected; we here conservatively assume a correlation coefficient of 0.7 among reaches. This conservatism also compensates for the fact that such features as diversions and hyporheic exchange are not otherwise accounted for in the integrator accuracy estimation. We applied MOI over the SWOT river network over the study area shown in Figure 8a, which amounts to all rivers which have mouths along the Alaska coastline. We chose this domain for two reasons: first, it includes both a large river (the Yukon) and many smaller rivers (e.g., the rivers north of the Yukon basin); we hypothesize that the integrators will reduce uncertainty for large rivers more so than small rivers, for both gage-constrained and unconstrained discharge. Second, this domain is a good example of an area with some gages (as shown in Figure 8a), but not the high density of gages in, for example, western Europe or CONUS, which is generally unrepresentative of the rest of the world.

To apply the integrator, we must specify values of uncertainty associated with SWOT observations, FLPs, and flow law approximation. Here we assume SWOT observation uncertainty as described in Section 3.2.3. We assume  $s_{bQ}Q^{-1}$  of 40%, which seems achievable for ungaged areas based on our reach-level experiments to date (Frasson et al., 2021). We assume  $\sigma_{Q_{FLA}}Q^{-1}$  of 5%. We note that gage measurements of river discharge have their own uncertainty (Kiang et al., 2018), and assume that mean annual flow computed from gages has an uncertainty of 5%; if actual discharge uncertainties are larger, constrained discharge uncertainty will be greater than that shown below.

##### 5.5.1. Random Discharge Uncertainty

Figures 8b–8d show the discharge uncertainty due to WSE, slope, and width uncertainty, respectively, and Figures 8e and 8f show the combined random discharge uncertainty. Figures 7b–7d show that observation errors generally lead to larger relative discharge uncertainty for smaller rivers; this is especially clear for WSE and width. Uncertainty for WSE and width remain below 0.15 (15%) throughout most of the domain and decrease with river width. Uncertainty for river slope differs, in that as rivers become flatter downstream, relative discharge error due

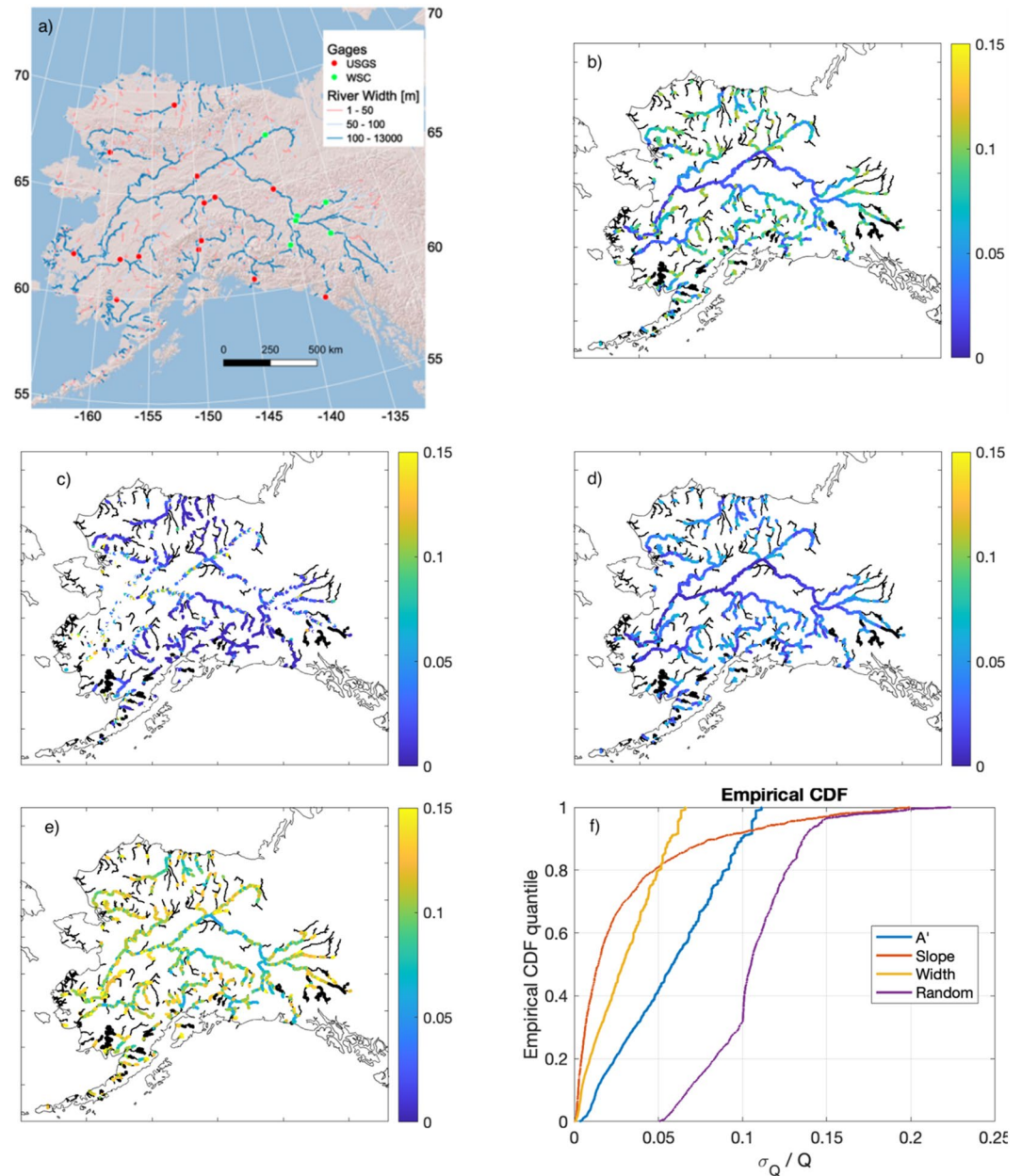


**Figure 8.** Study area and random error estimates. (a) River width and streamflow gages from the United States Geologic Survey (USGS) and the Water Survey of Canada (WSC) used to create the constrained discharge estimate and shaded relief. Relative random discharge errors ( $\sigma_{Q_{rand}} Q^{-1}$ ) errors due to (b) water surface elevation (WSE) (c) slope, and (d) width. (e) Total random discharge errors due to observations and flow law approximation error. (f) Cumulative distribution functions (CDFs) of random discharge error components and total. Axes (b)–(e) have nearly identical spatial extent to (a) and are unlabeled for simplicity.

to slope increases (compare Equation 4). The areas where no data are shown on the river network in Figure 8c are where a “low slope” algorithm will be used. For these reaches, we assume a rating curve form of the flow law and thus only keep the discharge uncertainty due to  $A'$ ; however, we assume that  $\sigma_{Q_{Struct}} Q^{-1}$  is twice as large (0.1), as we are using only  $WSE$  to approximate discharge, and thus ignoring changes in slope. Figure 7e for the total random uncertainty shows that random uncertainty no longer decreases for the largest rivers, because these large rivers are flat, and are expected to have larger flow law approximation error. The CDFs in Figure 8f show how these terms interact. Slope is the smallest factor in overall discharge uncertainty, for most (80%) of reaches. For the flatter reaches, slope tends to dominate, and is the only one of the three individual observation terms to

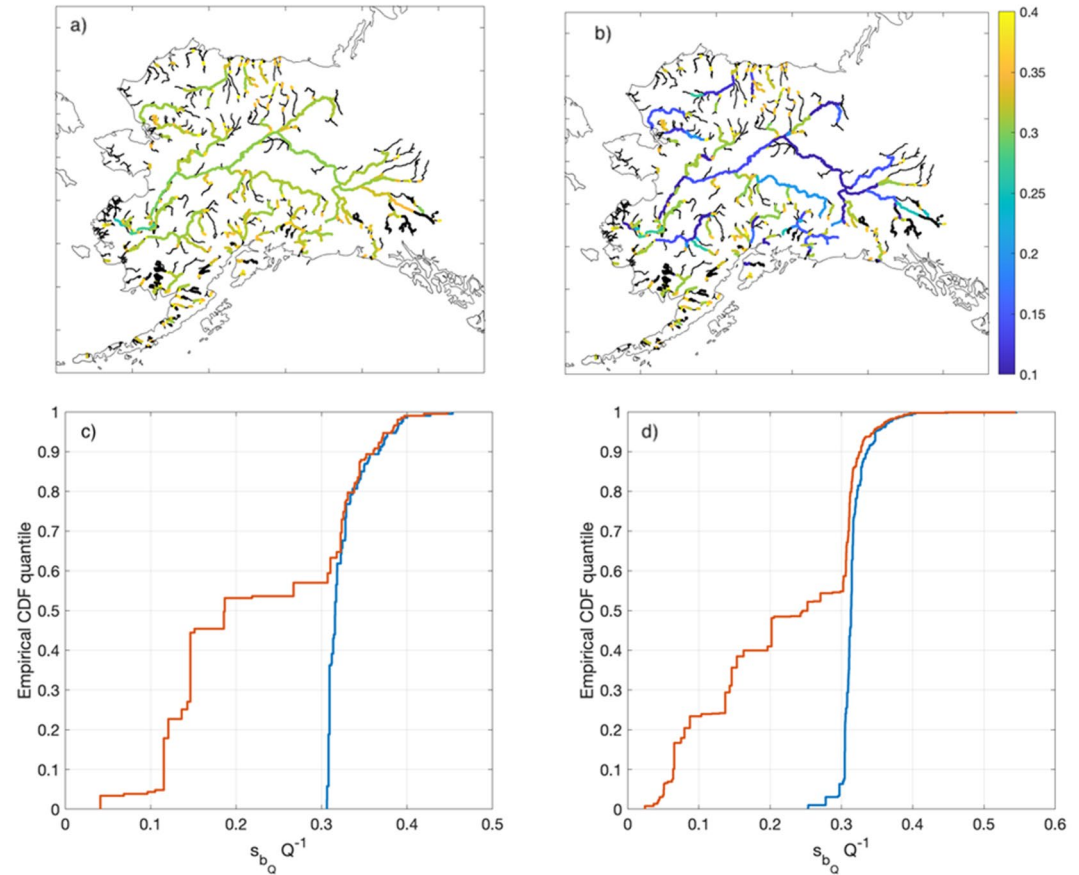


**Figure 9.** Systematic uncertainty,  $s_{b_Q}$ , over Alaska. Maps showing spatial variations in  $s_{b_Q}$  for the (a) unconstrained (b) constrained discharge estimates. The difference between unconstrained (blue) and constrained (red) values of  $s_{b_Q}$  for the (c) rivers north of the Yukon basin and (d) Yukon River basin. CDF, cumulative distribution function.

show a long tail. Indeed, the discharge uncertainties for  $A'$  and width are approximately linear in their CDFs, despite the underlying width data following the usual long-tail exponential distribution over the domain (Frasson et al., 2019). Combining the observation and flow law approximation error leads to the estimate of total random error  $\sigma_{Q_{rand}}Q^{-1}$ , which has a minimum value of 0.05, due to the minimum value of flow law approximation error assumed for all reaches. For approximately a third of reaches in the domain,  $\sigma_{Q_{rand}}Q^{-1}$  is dominated by  $A'$ , as indicated by the linear shape of the CDF up to the 0.3 quantile. Between 0.3 and 0.8,  $A'$  width and slope all play an important role in determining the final uncertainty. Above 0.8, slope dominates the reaches with highest random error are dominated by slope. Considering the total random error, the 67th percentile is 0.12, and the vast majority (>95%) of reaches have random error less than 0.15.

### 5.5.2. Systematic Discharge Uncertainty

Figure 9 shows the values of  $s_{b_Q}$  over the study domain. Figure 9a shows the unconstrained case: along the main-stem rivers, uncertainty predicted by MOI is 0.3, or a little lower, whereas on the smaller rivers upstream, uncertainty is closer to the assumed value of 0.4. Figure 9b shows the constrained case: note near gages, uncertainty reaches 0.05, matching the assumed value noted above. Figure 9c shows the comparison of the  $s_{b_Q}$  cdf for the Yukon River for the constrained and unconstrained cases. The effect of the gages is very stark: many reaches are either unconnected to rivers with gages or are located so far from the gage that the impact is relatively minimal; future work will present methods to compute the distance along river networks at which gage impact is minimal. Nonetheless, a little over half of the reaches in the Yukon basin benefit from the gages. Figure 9d shows the impact of gages on rivers north of the Yukon basin. Gages show a similar impact in this region: for both cases, the 67th percentile of  $s_{b_Q}$  is unchanged due to gages, whereas the median is reduced from 0.3 to 0.2, a 50% reduction.



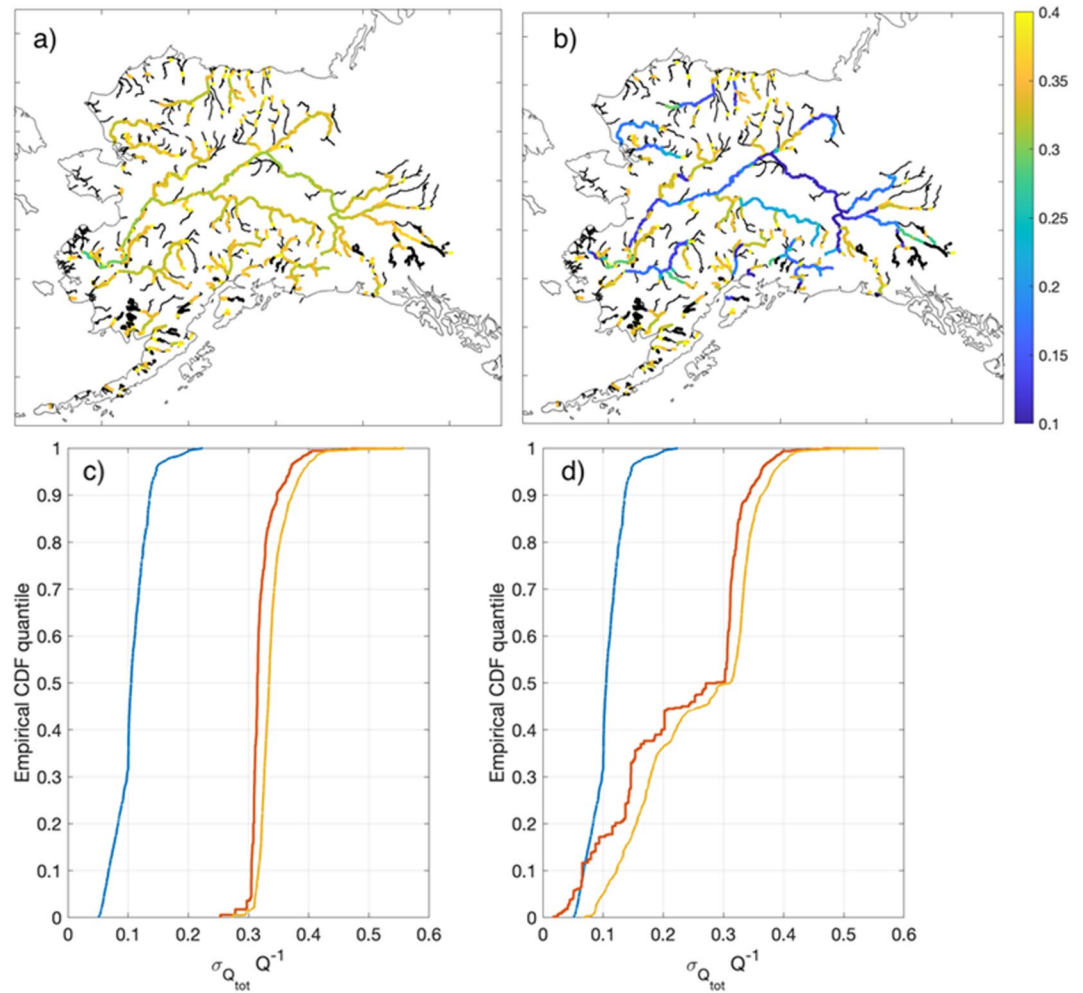


**Figure 10.** Maps of total uncertainty ( $\sigma_{Q_{tot}} Q^{-1}$ ), over Alaska for the (a) unconstrained (b) gage-constrained discharge estimates. Cumulative distribution functions (CDFs) of random (blue), systematic (red), and total uncertainty (gold) for the (c) unconstrained and (d) unconstrained discharge estimates.

### 5.5.3. Combined Discharge Uncertainty

Figure 10 shows the total uncertainty, combining both the  $s_{bQ}$  and  $\sigma_{Q_{rand}} Q^{-1}$ . Figures 10a and 10b show the stark contrast that adding gages has on the  $\sigma_{Q_{tot}} Q^{-1}$  discharge uncertainty: reaches with gages, and located further downstream generally have lower uncertainty for the constrained product. The uncertainty CDF for the unconstrained products (Figure 10c) shows that the systematic error due to parameters  $s_{bQ}$  dominates the total uncertainty in essentially all cases. This is still true most of the time for the gage-constrained case (Figure 10d):  $s_{bQ} > \sigma_{Q_{rand}}$  for 90% of the reaches in the domain.

This exercise to examine SWOT discharge uncertainty has illustrated three things. First, uncertainty is dominated by bias or systematic error. Second, the inclusion of gages means that the gage-constrained products will be able to provide nearly unbiased discharge for reaches that have gages or are located near gages. Third, the random error in SWOT discharge should be less than 15%; that is, time variations in discharge should be known within 15%, for the vast majority of reaches.

### 5.6. Comparing SWOT and Gage Discharge Uncertainty

We generally expect SWOT discharge accuracy to be somewhat lower than what is achieved from in situ measurements. We would not expect a gaged discharge time series to exhibit systematic bias that will likely be present with SWOT discharge estimates. On the other hand, gage discharge estimates have non-trivial

uncertainty as well. In their review, McMillan et al. (2012) present uncertainties from discharge predicted by a rating curve of at least 10%, with significantly higher uncertainty cited for special cases such as low flows, out-of-bank flows. Unsteady flow and complex geomorphology have also been found to lead to higher gaged uncertainties (Cheng et al., 2019). These values are consistent with other more recent studies (Coxon et al., 2015; Kiang et al., 2018; Sorengard & Di Baldassarre, 2017). Nonetheless, as noted above, systematic bias estimates of around 30% for  $s_{bQ}$  (see Section 5.5.2) are significantly larger than those reported for gaged discharge in the literature. SWOT measurements of discharge time variations  $\sim 15\%$  are expected to be somewhat greater than gaged discharge accuracy. Given the lack of gaged discharge in most parts of the world, a synergistic use of SWOT discharge, gaged discharge, and hydrologic models, with appropriate consideration of their respective uncertainties, seems the optimal way to advance our understanding of global hydrologic processes.

## 6. Conclusion

SWOT river discharge estimates will provide global discharge data for rivers wider than 100 m, including the world's largest ungaged basins. These discharge data have the potential to spark a revolution in global hydrologic science if their space-time sampling and uncertainty characteristics are accepted by the global community. SWOT discharge estimates will be created using relatively simple flow laws that combine SWOT measurements of WSE, width and slope, and FLP estimates. The observations will lead to approximate random uncertainty in SWOT discharge, on the order of 15%. Uncertainty in the FLPs will lead to systematic error that will express itself as bias in river discharge time series and will vary widely. For the “gage-constrained” branch of SWOT discharge estimates, mean flow is expected to be estimated within 20% for reaches that are near gages. Based on example results presented for Alaskan rivers, for the “unconstrained” branch of SWOT discharge, mean flow is expected to be within 30%. Results in other basins are expected to vary somewhat.

SWOT discharge estimates have the potential to lead to transformative new hydrologic science. Our study indicates that the combined random and systematic uncertainty for single pass discharge estimates can be as low or lower than 35% for most reaches, even when no gage data are used to constrain the SWOT discharge estimates. While calibrated hydrologic models can easily achieve this accuracy, in basins where no calibration data are available, this will be a significant improvement on global uncalibrated models (Emery et al., 2018). The temporal variations or anomaly in SWOT discharge will be estimated far more accurately than the total discharge with a random uncertainty of  $<15\%$  for most reaches, as we have shown, although the sparse sampling means that hydrographs may not be fully resolved (Sikder et al., 2021), especially for smaller and flashier rivers. The ability to accurately estimate streamflow variations implies that SWOT will provide accurate measurements of what amounts to the event flow hydrographs for all of the world's ungaged basins. Though available only for large rivers, and at temporal sampling on the order of 10 days on average, this will provide an important new resource for understanding global hydrological processes.

## Appendix A: Derivation of Modified Manning's Equation

The typical form of Manning's equation, for example, as presented by Sturm (2010) (see his equation. 4.9) is given by

$$V = \frac{1}{n} R^{2/3} S^{1/2} \quad (\text{A1})$$

where  $n$  is the coefficient representing the resistance of the river bank,  $V$  is the cross-sectional average velocity,  $S$  is the river slope, and  $R$  is the hydraulic radius, which is equal to the cross-sectional area divided by the wetted perimeter. The “river slope” is discussed in depth below. This equation was independently developed by multiple investigators.

Multiplying the cross-sectional area by the cross-sectional velocity yields the river discharge:

$$Q = AV = \frac{1}{n} A^{5/3} P^{-2/3} S^{1/2} \quad (\text{A2})$$

In rivers of the size that SWOT will see, the so-called “wide river” approximation yields very little error, typically <1% (Strelkoff & Clemmens, 2000). This allows substitution of river width ( $W$ ) for the wetted perimeter, which yields:

$$Q = \frac{1}{n} A^{5/3} W^{-2/3} S^{1/2} \quad (\text{A3})$$

### A1. Estimating River Cross-Sectional Area With SWOT

SWOT will measure the river width, river slope, and river WSE ( $H$ ), which form the basis of approximation of the cross-sectional area. Combining SWOT measurements of  $H$  and  $W$  allow measurements of the temporal changes in river cross-sectional area. Figure A1 shows a graphical representation of a time series of SWOT measurements. Visually, each successive SWOT measurement maps out a part of the cross-sectional shape. First, consider an example: visually from Figure A1, the change in cross-sectional area between, for example, the top two observations can be estimated using a trapezoidal shape, as described by Frasson (2021) and Durand et al. (2014). Extending this notion, the cross-sectional area above the lowest SWOT measurement can be estimated as a sum of the trapezoids from the lowest SWOT measurement to the desired time.

The previous paragraph illustrated the idea of approximating cross-sectional area using a time series of  $H$  and  $W$ . For SWOT applications, we take this idea one step further, defining an approach that is more robust to observation uncertainty. To calculate  $A$ , we first define  $A_0$ , the cross-sectional area below the lowest SWOT measurement. Consider a time series of SWOT observations of  $H_t$  and  $W_t$ , where the “ $t$ ” subscripts indicate that a quantity changes in time; an example time series is illustrated as a scatterplot of these two quantities in Figure A2. Next, define

$$A_t = A_0 + \delta A_t \quad (\text{A4})$$

where  $\delta A_t$  is the change in cross-sectional area between the overpass at time  $t$  and the lowest SWOT observation. Then  $\delta A_t$  can be computed by a simple integral over the height-width data, as described in Durand et al. (2014). Here, we note that  $\delta A_t$  can also be defined as an integral over a functional form that describes the response of  $W$  to  $H$ . To accommodate the noisy observations, we first fit a three-part piecewise-linear function to the  $H_t, W_t$  data (see Figure A2) and refer to this form as  $W = f(H)$ . Note that nonlinear forms could also be used to represent the response of width to changes in WSE; we have chosen a linear form here for simplicity. Then as shown by Durand et al. (2014),

$$\delta A_t = \int_{H_0}^{H_t} f(H) dH \quad (\text{A5})$$

where  $H_0$  is the WSE of the lowest flow observed by SWOT.

The final step in obtaining the form used by SWOT is motivated by having a cross-sectional area time series with zero median. Thus, we define the median cross-sectional area as the unknown, relating it to  $A_0$ . First define  $A'$ , the median-zero estimate of the cross-sectional area anomaly. Then  $A'_t$  can be calculated from  $\delta A_t$  via:

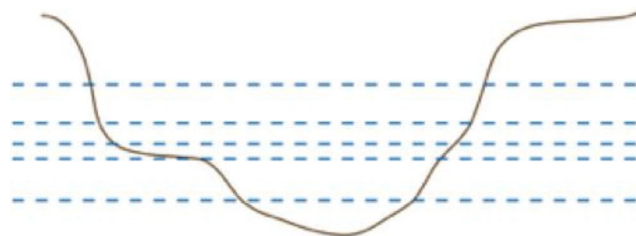


**Figure A1.** A notional river cross-section is shown, along with a notional time series of Surface Water and Ocean Topography (SWOT) measurements indicated by the dashed blue lines. Visually, each SWOT observation measures both the river water surface elevation ( $H$ ) and river width ( $W$ ). The time series of  $H$  and  $W$  can be used to approximate the cross-sectional area time series.

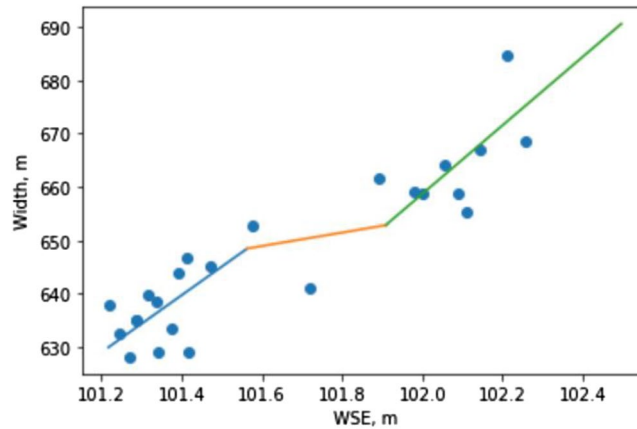


**Figure A2.** Simulated Surface Water and Ocean Topography (SWOT) measurements of water surface elevation (WSE) and river width, from a reach on the Ohio River (blue points). The three line segments represent a piecewise linear function that represents the relationship between WSE and width.

$$A'_t = \delta A_t - \delta A_{shift} \quad (A6)$$

where  $\delta A_{shift}$  is the median of the  $\delta A_t$  time series. This leads to the final approximation of cross-sectional area:

$$A_t = A'_t + \bar{A} \quad (A7)$$

Thus, we have approximated the cross-sectional area at any time based on the median cross-sectional area  $\bar{A}$  and the time-series anomaly  $A'_t$ , and  $\bar{A}$  is the unobserved flow law parameter to be estimated using methods described in Section 4.3. Substituting Equation A7 into Equation A3 yields Equation 1, the modified Manning equation discussed in the manuscript.

We treat  $A'_t$  as being measured, because it is estimated in a direct way from basic SWOT measurements  $H_t$ ,  $W_t$ . The measurement uncertainty of  $A'_t$  can be computed from simpler estimate of cross-sectional area change:

$$\hat{A}'_t = (H_t - \bar{H}) \left( \frac{W_t + \bar{W}}{2} \right) \quad (A8)$$

where  $\bar{H}$ ,  $\bar{W}$  are the height and width measurements at the median WSE, and  $\hat{A}'_t$  has the same basic definition as  $A'_t$ , but is estimated in a different way. Indeed,  $\hat{A}'_t$  would be expected to be less precise than  $A'_t$ , since it is computed using only two observations. Thus, a conservative estimate of the uncertainty of  $A'_t$  can be computed based on Equation A8:

$$\sigma_{A'} = \sigma_H W_t \sqrt{2} \quad (A9)$$

## A2. Using River Surface Slope in Manning's Equation for SWOT Discharge

Manning's equation, as given in Equation A1, usually is recommended only to apply in contexts where the slope of the river bed is equal to the slope of the river surface (often referred to as “uniform flow”). More generally, the modified Manning's equation assumes that the so-called friction slope or rate of momentum loss downstream is equal to the slope of the water surface. It does *not* assume that the bed slope and surface slope are identical, and thus it does *not* assume uniform flow (Tuozzolo, Langhorst, et al., 2019). The surface slope represents the sum of two forces acting on the water: the downward pull of gravity, and the spatial gradient in hydrostatic forces, represented as downstream changes in river depth. Thus, Equation 1 corresponds exactly to the steady state equilibrium of the “diffusion wave” approximation (Trigg et al., 2009). Garambois and Monnier (2015) provide an objective basis for the modified Manning's equation by showing that it results from neglecting the acceleration terms in the shallow water equations with the assumption that Froude numbers are low (i.e., <0.3). Garambois

and Monnier (2015) suggested that the modified Manning's equation is thus a “low Froude approximation”. Most rivers that SWOT can measure will have Froude  $<0.3$ , most of the time: for example, see Bjerklie et al. (2020), which makes this approximation reasonable. However, even if Froude numbers are significantly higher than 0.3, the modified Manning equation can be expected to function adequately in most cases as it has several degrees of freedom with which to fit the data. In other words,  $Fr < 0.3$  is a sufficient condition to justify the modified Manning formulation, but it is not necessary. Nonetheless, care must be taken not to apply the modified Manning's equation in parts of the river such as riffles or low-head dams where there is a significant elevation drop across a very short distance where flow is expected to be supercritical. This is handled for SWOT discharge by using a database of such structures within SWORD to define reach boundaries that exclude such structures. The length of river that includes the hydraulic structure is defined as a “dam reach” (Altenau et al., 2021), a special class of reach for which WSE, width, slope, and discharge are not computed. Similarly, lakes on SWOT rivers are expected to have a surface slope too low to resolve; discharge is not computed for lakes (Altenau et al., 2021).

### Acronyms

CDF	cumulative distribution function
FLP	flow law parameter
FLPE	flow law parameter estimation
geoBAM	Geomorphically informed Bayesian At many stations hydraulic geometry- Manning Algorithm
GRADES	Global Reach-Level A Priori Discharge Estimates for SWOT
McFLI	Mass Conserved Flow Law Inversion
MOI	Mean Optimization Integrator
SoS	SWORD of Science
SWORD	SWOT mission river database
SWOT	Surface Water and Ocean Topography
USGS	United States Geological Survey
WBM	Water Balance Model
WSC	Water Survey of Canada
WSE	water surface elevation

### Data Availability Statement

The data chain used for the confluence run example (Section 4.4) is available on Zenodo (<https://doi.org/10.5281/zenodo.7392075>).

### References

- Adams, T. E., Chen, S., & Dymond, R. (2018). Results from operational hydrologic forecasts using the NOAA/NWS OHRFC Ohio River Community HEC-RAS model. *Journal of Hydrologic Engineering*, 23(7), 1–17. [https://doi.org/10.1061/\(ASCE\)HE.1943-5584.0001663](https://doi.org/10.1061/(ASCE)HE.1943-5584.0001663)
- Allen, G. H., & Pavelsky, T. M. (2018). Global extent of rivers and streams. *Science*, 361(6402), 585–587. <https://doi.org/10.1126/science.aat0636>
- Altenau, E. H., Pavelsky, T. M., Durand, M. T., Yang, X., Frasson, R. P. D., & Bendezu, L. (2021). The Surface Water and Ocean Topography (SWOT) Mission River Database (SWORD): A global river network for satellite data products. *Water Resources Research*, 57(7), e2021WR030054. <https://doi.org/10.1029/2021WR030054>
- Altenau, E. H., Pavelsky, T. M., Moller, D., Pitcher, L. H., Bates, P. D., Durand, M. T., & Smith, L. C. (2019). Temporal variations in river water surface elevation and slope captured by AirSWOT. *Remote Sensing of Environment*, 224, 304–316. <https://doi.org/10.1016/j.rse.2019.02.002>
- Andreadis, K. M., Brinkerhoff, C. B., & Gleason, C. J. (2020). Constraining the assimilation of SWOT observations with hydraulic geometry relations. *Water Resources Research*, 56(5), e2019WR026611. <https://doi.org/10.1029/2019WR026611>
- Andreadis, K. M., Clark, E. A., Lettenmaier, D. P., & Alsdorf, D. E. (2007). Prospects for river discharge and depth estimation through assimilation of swath-altimetry into a raster-based hydrodynamics model. *Geophysical Research Letters*, 34(10), L10403. <https://doi.org/10.1029/2007gl029721>
- Beck, H. E., de Roo, A., & van Dijk, A. I. J. M. (2015). Global maps of streamflow characteristics based on observations from several thousand catchments. *Journal of Hydrometeorology*, 16(4), 1478–1501. <https://doi.org/10.1175/Jhm-D-14-0155.1>
- Biancamaria, S., Durand, M., Andreadis, K. M., Bates, P. D., Boone, A., Mognard, N. M., et al. (2011). Assimilation of virtual wide swath altimetry to improve Arctic river modeling. *Remote Sensing of Environment*, 115(2), 373–381. <https://doi.org/10.1016/j.rse.2010.09.008>
- Biancamaria, S., Lettenmaier, D. P., & Pavelsky, T. M. (2016). The SWOT mission and its capabilities for land hydrology. *Surveys in Geophysics*, 37(2), 303–337. <https://doi.org/10.1007/s10712-015-9346-y>
- Bjerklie, D. M., Birkett, C. M., Jones, J. W., Carabajal, C., Rover, J. A., Fulton, J. W., & Garabois, P. A. (2018). Satellite remote sensing estimation of river discharge: Application to the Yukon River Alaska. *Journal of Hydrology*, 561, 1000–1018. <https://doi.org/10.1016/j.jhydrol.2018.04.005>

### Acknowledgments

R. P. M. Frasson, C. H. David, and C. Stuurman were supported by the Jet Propulsion Laboratory, California Institute of Technology, under a contract with the U.S. National Aeronautics and Space Administration. Teams at Kansas State University, Ohio State University, and the University of Massachusetts were supported by NASA SWOT Science Team Grants 80NSSC20K1143, 80NSSC20K1141, and 80NSSC20K1339, respectively. Paul Bates was supported by a Royal Society Wolfson Research Merit award. H. Oubanas and P.-O. Malaterre were supported by CNES under the TOSCA-CNES DAHM contract. The authors would like to acknowledge Whitney Baxter for creating the original art shown in Figures 1, 2, and 6. Jeff Dozier, Jack Eggleston, and two anonymous reviewers greatly improved the quality of the manuscript. Confluence input and output data are available at <https://zenodo.org/record/7392075#.Y43vrC-B2wA>. Any use of trade, firm, or product names is for descriptive purposes only and does not imply endorsement by the US Government.

- Bjerklie, D. M., Dingman, S. L., & Bolster, C. H. (2005). Comparison of constitutive flow resistance equations based on the Manning and Chezy equations applied to natural rivers. *Water Resources Research*, 41(11), W11502. <https://doi.org/10.1029/2004wr003776>
- Bjerklie, D. M., Fulton, J. W., Dingman, S. L., Canova, M. G., Minear, J. T., & Moramarco, T. (2020). Fundamental hydraulics of cross sections in natural rivers: Preliminary analysis of a large data set of acoustic Doppler flow measurements. *Water Resources Research*, 56(3), e2019WR025986. <https://doi.org/10.1029/2019WR025986>
- Bonnema, M. G., Sikder, S., Hossain, F., Durand, M., Gleason, C. J., & Bjerklie, D. M. (2016). Benchmarking wide swath altimetry-based river discharge estimation algorithms for the Ganges river system. *Water Resources Research*, 52(4), 2439–2461. <https://doi.org/10.1002/2015wr017296>
- Brinkerhoff, C. B., Gleason, C. J., Feng, D., & Lin, P. (2020). Constraining remote river discharge estimation using reach-scale geomorphology. *Water Resources Research*, 56(11), e2020WR027949. <https://doi.org/10.1029/2020WR027949>
- Brinkerhoff, C. B., Gleason, C. J., & Ostendorf, D. W. (2019). Reconciling at-a-station and at-many-stations hydraulic geometry through river-wide geomorphology. *Geophysical Research Letters*, 46(16), 9637–9647. <https://doi.org/10.1029/2019gl084529>
- Cheng, Z. Y., Lee, K., Kim, D., Muste, M., Vidmar, P., & Hulme, J. (2019). Experimental evidence on the performance of rating curves for continuous discharge estimation in complex flow situations. *Journal of Hydrology*, 568, 959–971. <https://doi.org/10.1016/j.jhydrol.2018.11.021>
- Cohen, S., Kettner, A. J., & Syvitski, J. P. M. (2014). Global suspended sediment and water discharge dynamics between 1960 and 2010: Continental trends and intra-basin sensitivity. *Global and Planetary Change*, 115, 44–58. <https://doi.org/10.1016/j.gloplacha.2014.01.011>
- Coss, S., Durand, M., Gleason, C., Tebaldi, N., & Simmons, T. (2022). A framework for estimating global river discharge from the Surface Water and Ocean Topography satellite mission example data (Version 2) [Dataset]. Zenodo. <https://doi.org/10.5281/zenodo.7392075>
- Coxon, G., Freer, J., Westerberg, I. K., Wagener, T., Woods, R., & Smith, P. J. (2015). A novel framework for discharge uncertainty quantification applied to 500 UK gauging stations. *Water Resources Research*, 51(7), 5531–5546. <https://doi.org/10.1002/2014wr016532>
- Dingman, S. L. (2007). Analytical derivation of at-a-station hydraulic-geometry relations. *Journal of Hydrology*, 334(1–2), 17–27. <https://doi.org/10.1016/j.jhydrol.2006.09.021>
- Durand, M., Chen, C., Frasson, R. P. D., Pavelsky, T. M., Williams, B., Yang, X., & Fore, A. (2020). How will radar layover impact SWOT measurements of water surface elevation and slope, and estimates of river discharge? *Remote Sensing of Environment*, 247, 111883. <https://doi.org/10.1016/j.rse.2020.111883>
- Durand, M., Gleason, C. J., Garambois, P. A., Bjerklie, D., Smith, L. C., Roux, H., et al. (2016). An intercomparison of remote sensing river discharge estimation algorithms from measurements of river height, width, and slope. *Water Resources Research*, 52(6), 4527–4549. <https://doi.org/10.1002/2015wr018434>
- Durand, M., Neal, J., Rodriguez, E., Andreadis, K. M., Smith, L. C., & Yoon, Y. (2014). Estimating reach-averaged discharge for the River Severn from measurements of river water surface elevation and slope. *Journal of Hydrology*, 511, 92–104. <https://doi.org/10.1016/j.jhydrol.2013.12.050>
- Durand, M., Rodriguez, E., Alsdorf, D. E., & Trigg, M. (2010). Estimating river depth from remote sensing swath interferometry measurements of river height, slope, and width. *IEEE Journal of Selected Topics in Applied Earth Observations and Remote Sensing*, 3(1), 20–31. <https://doi.org/10.1109/Jstars.2009.2033453>
- Emery, C. M., David, C. H., Andreadis, K. M., Turmon, M. J., Reager, J. T., Hobbs, J. M., et al. (2020). Underlying fundamentals of Kalman filtering for river network modeling. *Journal of Hydrometeorology*, 21(3), 453–474. <https://doi.org/10.1175/Jhm-D-19-0084.1>
- Emery, C. M., Paris, A., Biancamaria, S., Boone, A., Calmant, S., Garambois, P. A., & da Silva, J. S. (2018). Large-scale hydrological model river storage and discharge correction using a satellite altimetry-based discharge product. *Hydrology and Earth System Sciences*, 22(4), 2135–2162. <https://doi.org/10.5194/hess-22-2135-2018>
- Ferguson, R. (2010). Time to abandon the Manning equation? *Earth Surface Processes and Landforms*, 35(15), 1873–1876. <https://doi.org/10.1002/esp.2091>
- Fjortoft, R., Gaudin, J. M., Lalaurie, J. C., Mallet, A., Nouvel, J. F., Martinot-Lagarde, J., et al. (2014). KaRIn on SWOT: Characteristics of near-nadir Ka-band interferometric SAR imagery. *IEEE Transactions on Geoscience and Remote Sensing*, 52(4), 2172–2185. <https://doi.org/10.1109/tgrs.2013.2258402>
- Frasson, R. P. d. M. (2021). Using the Surface Water and Ocean Topography mission data to estimate river bathymetry and channel roughness. In G. J.-P. Schumann (Ed.), *Earth observation for flood applications: Progress and perspectives* (1st ed., pp. 398). Elsevier. <https://doi.org/10.1016/B978-0-12-819412-6.00005-5>
- Frasson, R. P. d. M., Durand, M. T., Larnier, K., Gleason, C., Andreadis, K. M., Hagemann, M., et al. (2021). Exploring the factors controlling the error characteristics of the Surface Water and Ocean Topography mission discharge estimates. *Water Resources Research*, 57(6), e2020WR028519. <https://doi.org/10.1029/2020WR028519>
- Frasson, R. P. D., Pavelsky, T. M., Fonstad, M. A., Durand, M. T., Allen, G. H., Schumann, G., et al. (2019). Global relationships between River Width, slope, catchment area, Meander Wavelength, Sinuosity, and discharge. *Geophysical Research Letters*, 46(6), 3252–3262. <https://doi.org/10.1029/2019gl082027>
- Frasson, R. P. D., Wei, R., Durand, M., Minear, J. T., Domeneghetti, A., Schumann, G., et al. (2017). Automated river reach definition strategies: Applications for the Surface Water and Ocean Topography mission. *Water Resources Research*, 53(10), 8164–8186. <https://doi.org/10.1002/2017wr020887>
- Garambois, P. A., & Monnier, J. (2015). Inference of effective river properties from remotely sensed observations of water surface. *Advances in Water Resources*, 79, 103–120. <https://doi.org/10.1016/j.advwatres.2015.02.007>
- Getirana, A., Kumar, S., Giroto, M., & Rodell, M. (2017). Rivers and floodplains as key components of global terrestrial water storage variability. *Geophysical Research Letters*, 44(20), 10359–10368. <https://doi.org/10.1002/2017gl074684>
- Gleason, C. J., & Durand, M. T. (2020). Remote sensing of river discharge: A review and a framing for the discipline. *Remote Sensing*, 12(7), 1107. <https://doi.org/10.3390/rs12071107>
- Gleason, C. J., Garambois, P. A., & Durand, M. (2017). *Tracking river flows from space* (Vol. 98). Eos.
- Gleason, C. J., & Hamdan, A. N. (2017). Crossing the (watershed) divide: Satellite data and the changing politics of international river basins. *Geographical Journal*, 183(1), 2–15. <https://doi.org/10.1111/geoj.12155>
- Gleason, C. J., & Smith, L. C. (2014). Toward global mapping of river discharge using satellite images and at-many-stations hydraulic geometry. *Proceedings of the National Academy of Sciences of the United States of America*, 111(13), 4788–4791. <https://doi.org/10.1073/pnas.1317606111>
- Gleason, C. J., Smith, L. C., & Lee, J. (2014). Retrieval of river discharge solely from satellite imagery and at-many-stations hydraulic geometry: Sensitivity to river form and optimization parameters. *Water Resources Research*, 50(12), 9604–9619. <https://doi.org/10.1002/2014wr016109>

- Gualtieri, P., De Felice, S., Pasquino, V., & Doria, G. P. (2018). Use of conventional flow resistance equations and a model for the Nikuradse roughness in vegetated flows at high submergence. *Journal of Hydrology and Hydromechanics*, 66(1), 107–120. <https://doi.org/10.1515/johh-2017-0028>
- Hagemann, M. W., Gleason, C. J., & Durand, M. T. (2017). BAM: Bayesian AMHG-Manning inference of discharge using remotely sensed stream width, slope, and height. *Water Resources Research*, 53(11), 9692–9707. <https://doi.org/10.1002/2017wr021626>
- Hannah, D. M., Demuth, S., van Lanen, H. A. J., Looser, U., Prudhomme, C., Rees, G., et al. (2011). Large-scale river flow archives: Importance, current status and future needs. *Hydrological Processes*, 25(7), 1191–1200. <https://doi.org/10.1002/hyp.7794>
- Hou, A. Y., Kakar, R. K., Neeck, S., Azarbarzin, A. A., Kummerow, C. D., Kojima, M., et al. (2014). The global precipitation measurement mission. *Bulletin of the American Meteorological Society*, 95(5), 701–722. <https://doi.org/10.1175/Bams-D-13-00164.1>
- Huffman, G. J., Bolvin, D. T., Braithwaite, D., Hsu, K. L., Joyce, R. J., Kidd, C., et al. (2020). Integrated multi-satellite retrievals for the global precipitation measurement (GPM) mission (IMERG). In V. Levizzani, C. Kidd, D. Kirschbaum, K. Kummerow, K. Nakamura, & F. J. Turk (Eds.), *Satellite precipitation measurement*, (Vol. 1, pp. 343–353).
- Ishitsuka, Y., Gleason, C. J., Hagemann, M. W., Beighley, E., Allen, G. H., Feng, D. M., et al. (2021). Combining optical remote sensing, McFLI discharge estimation, global hydrologic modeling, and data assimilation to improve daily discharge estimates across an entire large watershed. *Water Resources Research*, 57(3), e2020WR027794. <https://doi.org/10.1029/2020WR027794>
- JPL Internal Document. (2017). *SWOT project mission performance and error budget*. California Institute of Technology. Retrieved from [https://swot.jpl.nasa.gov/system/documents/files/2178\\_2178\\_SWOT\\_D-79084\\_v10Y\\_FINAL\\_REVA\\_06082017.pdf](https://swot.jpl.nasa.gov/system/documents/files/2178_2178_SWOT_D-79084_v10Y_FINAL_REVA_06082017.pdf)
- JPL Internal Document. (2018). *SWOT project science requirements document*. California Institute of Technology. Retrieved from [https://swot.jpl.nasa.gov/system/documents/files/2176\\_2176\\_D-61923\\_SRD\\_Rev\\_B\\_20181113.pdf](https://swot.jpl.nasa.gov/system/documents/files/2176_2176_D-61923_SRD_Rev_B_20181113.pdf)
- JPL Internal Document. (2020). *SWOT product description: Level 2 KaRIn high rate river single pass vector product*. California Institute of Technology. Retrieved from [https://podaac-tools.jpl.nasa.gov/drive/files/misc/web/misc/swot\\_mission\\_docs/pdd/D-56413\\_SWOT\\_Product\\_Description\\_L2\\_HR\\_RiverSP\\_20200825a.pdf](https://podaac-tools.jpl.nasa.gov/drive/files/misc/web/misc/swot_mission_docs/pdd/D-56413_SWOT_Product_Description_L2_HR_RiverSP_20200825a.pdf)
- Kiang, J. E., Gazoorian, C., McMillan, H., Coxon, G., Le Coz, J., Westerberg, I. K., et al. (2018). A comparison of methods for streamflow uncertainty estimation. *Water Resources Research*, 54(10), 7149–7176. <https://doi.org/10.1029/2018wr022708>
- Larnier, K., Monnier, J., Garambois, P. A., & Verley, J. (2020). River discharge and bathymetry estimation from SWOT altimetry measurements. *Inverse Problems in Science and Engineering*, 29(6), 759–789. <https://doi.org/10.1080/17415977.2020.1803858>
- Li, D. Y., Andreadis, K. M., Margulis, S. A., & Lettenmaier, D. P. (2020). A data assimilation framework for generating space-time continuous daily SWOT river discharge data products. *Water Resources Research*, 56(6), e2019WR026999. <https://doi.org/10.1029/2019WR026999>
- Lin, P. R., Pan, M., Beck, H. E., Yang, Y., Yamazaki, D., Frasson, R., et al. (2019). Global reconstruction of naturalized river flows at 2.94 million reaches. *Water Resources Research*, 55(8), 6499–6516. <https://doi.org/10.1029/2019wr025287>
- McMillan, H., Krueger, T., & Freer, J. (2012). Benchmarking observational uncertainties for hydrology: Rainfall, river discharge and water quality. *Hydrological Processes*, 26, 4078–4111. <https://doi.org/10.1002/hyp.9384>
- Nickles, C., Beighley, E., Durand, M., & Frasson, R. P. D. (2020). Integrating lateral inflows into a SWOT mission river discharge algorithm. *Water Resources Research*, 56(10), e2019WR026589. <https://doi.org/10.1029/2019WR026589>
- Oubanas, H., Gejadze, I., Malaterre, P. O., Durand, M., Wei, R., Frasson, R. P. M., & Domeneghetti, A. (2018). Discharge estimation in ungauged basins through variational data assimilation: The potential of the SWOT mission. *Water Resources Research*, 54(3), 2405–2423. <https://doi.org/10.1002/2017wr021735>
- Paiva, R. C. D., Durand, M. T., & Hossain, F. (2015). Spatiotemporal interpolation of discharge across a river network by using synthetic SWOT satellite data. *Water Resources Research*, 51(1), 430–449. <https://doi.org/10.1002/2014wr015618>
- Pavelsky, T. M., Durand, M. T., Andreadis, K. M., Beighley, R. E., Paiva, R. C. D., Allen, G. H., & Miller, Z. F. (2014). Assessing the potential global extent of SWOT river discharge observations. *Journal of Hydrology*, 519, 1516–1525. <https://doi.org/10.1016/j.jhydrol.2014.08.044>
- Pavelsky, T. M., & Smith, L. C. (2008). RivWidth: A software tool for the calculation of river widths from remotely sensed imagery. *IEEE Geoscience and Remote Sensing Letters*, 5(1), 70–73. <https://doi.org/10.1109/LGRS.2007.908305>
- Pavlis, N. K., Holmes, S. A., Kenyon, S. C., & Factor, J. K. (2012). The development and evaluation of the Earth Gravitational Model 2008 (EGM2008). *Journal of Geophysical Research*, 117(B4), 1–38. <https://doi.org/10.1029/2011JB008916>
- Povey, A. C., & Grainger, R. G. (2015). Known and unknown unknowns: Uncertainty estimation in satellite remote sensing. *Atmospheric Measurement Techniques*, 8(11), 4699–4718. <https://doi.org/10.5194/amt-8-4699-2015>
- Riggs, R. M., Allen, G. H., Wang, J., & Sikder, M. S. (2022). *Using SWOT observed lake storage change to constrain river inflow and outflow discharge*. American Geophysical Union.
- Rodriguez, E., Durand, M., & Frasson, R. P. D. (2020). Observing rivers with varying spatial scales. *Water Resources Research*, 56(9), e2019WR026476. <https://doi.org/10.1029/2019WR026476>
- Sikder, M. S., Bonnema, M., Emery, C. M., David, C. H., Lin, P. R., Pan, M., et al. (2021). A synthetic data set inspired by satellite altimetry and impacts of sampling on global spaceborne discharge characterization. *Water Resources Research*, 57(2), e2020WR029035. <https://doi.org/10.1029/2020WR029035>
- Smith, R. C. (2013). *Uncertainty quantification: Theory, implementation, and applications*. Society for Industrial and Applied Mathematics.
- Sorengard, M., & Di Baldassarre, G. (2017). Simple vs complex rating curves: Accounting for measurement uncertainty, slope ratio and sample size. *Hydrological Sciences Journal-Journal Des Sciences Hydrologiques*, 62(13), 2072–2082. <https://doi.org/10.1080/02626667.2017.1367397>
- Strelkoff, T. S., & Clemmens, A. J. (2000). Approximating wetted perimeter in power-law cross section. *Journal of Irrigation and Drainage Engineering*, 126(2), 98–109. [https://doi.org/10.1061/\(ASCE\)0733-9437\(2000\)126:2\(98\)](https://doi.org/10.1061/(ASCE)0733-9437(2000)126:2(98))
- Sturm, T. (2010). *Open channel hydraulics* (2nd ed.). McGraw Hill Higher Education.
- Trigg, M. A., Wilson, M. D., Bates, P. D., Horritt, M. S., Alsdorf, D. E., Forsberg, B. R., & Vega, M. C. (2009). Amazon flood wave hydraulics. *Journal of Hydrology*, 374(1–2), 92–105. <https://doi.org/10.1016/j.jhydrol.2009.06.004>
- Tuozzolo, S., Langhorst, T., Frasson, R. P. D. M., Pavelsky, T., Durand, M., & Schobelock, J. J. (2019). The impact of reach averaging Manning's equation for an in-situ dataset of water surface elevation, width, and slope. *Journal of Hydrology*, 578, 123866. <https://doi.org/10.1016/j.jhydrol.2019.06.038>
- Tuozzolo, S., Lind, G., Overstreet, B., Mangano, J., Fonstad, M., Hagemann, M., et al. (2019). Estimating river discharge with swath altimetry: A proof of concept using AirSWOT observations. *Geophysical Research Letters*, 46(3), 1459–1466. <https://doi.org/10.1029/2018gl080771>
- Turnipseed, D. P., & Sauer, V. B. (2010). Discharge measurements at gaging stations. *U.S. Geological Survey Techniques and Methods Book*, 3, 87.
- Wang, J., Riggs, R. M., Allen, G. H., Sikder, M. S., Durand, M. T., Gleason, C. J., & Pavelsky, T. (2021). *Preliminary results for "Lakeflow", an algorithm to improve SWOT flow-law parameters through integrating river-lake mass conservation. H121-05: Surface Water Hydrology from SWOT, NISAR, and ICESat-2 II eLightning*. American Geophysical Union.

- Whittemore, A., Ross, M. R. V., Dolan, W., Langhorst, T., Yang, X., Pawar, S., et al. (2020). A participatory science approach to expanding instream infrastructure inventories. *Earth's Future*, 8(11), e2020EF001558. <https://doi.org/10.1029/2020EF001558>
- Wongchuig-Correa, S., de Paiva, R. C. D., Biancamaria, S., & Collischonn, W. (2020). Assimilation of future SWOT-based river elevations, surface extent observations and discharge estimations into uncertain global hydrological models. *Journal of Hydrology*, 590, 125473. <https://doi.org/10.1016/j.jhydrol.2020.125473>
- Xin, A. (2022). *Examining the premise of the "LakeFlow" discharge algorithm in the contiguous United States*. Thesis of Master of Science. Kansas State University. Retrieved from <https://hdl.handle.net/2097/42460>
- Yamazaki, D., Ikeshima, D., Sosa, J., Bates, P. D., Allen, G. H., & Pavelsky, T. M. (2019). MERIT Hydro: A high-resolution global hydrography map based on latest topography dataset. *Water Resources Research*, 55(6), 5053–5073. <https://doi.org/10.1029/2019wr024873>
- Yamazaki, D., Kanae, S., Kim, H., & Oki, T. (2011). A physically based description of floodplain inundation dynamics in a global river routing model. *Water Resources Research*, 47(4), W04501. <https://doi.org/10.1029/2010wr009726>
- Yang, X., Pavelsky, T. M., & Allen, G. H. (2020). The past and future of global river ice. *Nature*, 577(7788), 69–73. <https://doi.org/10.1038/s41586-019-1848-1>
- Yang, X., Pavelsky, T. M., Ross, M. R. V., Januchowski-Hartley, S. R., Dolan, W., Altenau, E. H., et al. (2022). Mapping flow-obstructing structures on global rivers. *Water Resources Research*, 58(1), e2021WR030386. <https://doi.org/10.1029/2021wr030386>
- Yang, Y., Lin, P., Fisher, C. K., Turmon, M., Hobbs, J., Emery, C. M., et al. (2019). Enhancing SWOT discharge assimilation through spatiotemporal correlations. *Remote Sensing of Environment*, 234, 111450. <https://doi.org/10.1016/j.rse.2019.111450>
- Yoon, Y., Durand, M., Merry, C. J., Clark, E. A., Andreadis, K. M., & Alsdorf, D. E. (2012). Estimating river bathymetry from data assimilation of synthetic SWOT measurements. *Journal of Hydrology*, 464, 363–375. <https://doi.org/10.1016/j.jhydrol.2012.07.028>
- Yoon, Y., Garambois, P. A., Paiva, R. C. D., Durand, M., Roux, H., & Beighley, E. (2016). Improved error estimates of a discharge algorithm for remotely sensed river measurements: Test cases on Sacramento and Garonne Rivers. *Water Resources Research*, 52(1), 278–294. <https://doi.org/10.1002/2015wr017319>
- Zhao, G., & Gao, H. L. (2019). Estimating reservoir evaporation losses for the United States: Fusing remote sensing and modeling approaches. *Remote Sensing of Environment*, 226, 109–124. <https://doi.org/10.1016/j.rse.2019.03.015>

## Erratum

In the originally published version of this article, affiliations 20 and 25 were duplicates. Jida Wang's affiliation number has been changed from 25 to 20, and the repeated affiliation, “<sup>25</sup>Department of Geography and Geospatial Sciences, Kansas State University, Manhattan, KS, USA,” has been removed. This error has been corrected, and this may be considered the authoritative version of record.